

## ORIGIN OF BIMODALITY IN GALAXY PROPERTIES: COLD AND HOT FLOWS, CLUSTERING AND FEEDBACK

AVISHAI DEKEL & YUVAL BIRNBOIM

Racah Institute of Physics, The Hebrew University, Jerusalem Israel

*Draft version February 7, 2020*

### ABSTRACT

We address the origin of the robust bi-modality observed in galaxy properties about a characteristic stellar mass  $\sim 3 \times 10^{10} M_{\odot}$ . Less massive galaxies tend to be ungrouped *blue* star-forming disks, with properties correlated along a “fundamental line”. More massive galaxies are typically grouped *red* old-star spheroids on a “fundamental plane” and hosting AGNs.  $M/L$  is at a minimum near the critical mass. Color-magnitude data show a gap between the red and blue sequences, extremely red luminous galaxies already at  $z \sim 1$ , a truncation of today’s blue sequence above  $L_*$ , and massive starbursts at  $z \sim 2$ -4.

We propose that these bi-modality features are driven by the *thermal* properties of the inflowing gas and their interplay with the *clustering* and *feedback* processes, all functions of the dark-matter halo mass and associated with a similar characteristic scale. In halos below a critical shock-heating mass  $M_{\text{shock}} \sim 6 \times 10^{11} M_{\odot}$ , disks are built by *cold streams*, not heated by a virial shock, yielding efficient early star formation (SFR). It is regulated by supernova and radiative feedbacks into a long sequence of bursts in blue galaxies constrained to the fundamental line. Cold streams penetrating through hot media in  $> M_{\text{shock}}$  halos at  $z \geq 2$  lead to massive starbursts in  $> L_*$  galaxies. At  $z < 2$ , in  $> M_{\text{shock}}$  halos hosting groups, the gas is heated by a virial shock, and being dilute it becomes vulnerable to feedback from energetic sources such as AGNs. This shuts off gas supply and prevents further star formation, preferentially in spheroids formed by mergers in groups. Subsequent passive evolution leads to “red-and-dead” massive spheroids starting at  $z \sim 1$ . The SFR is high just below  $M_{\text{shock}}$ , where the feedbacks are weak, leading to a minimum in  $M/L$ . Convolved with the clustering scale growth, this explains the observed SFR broad peak at  $z \gtrsim 1$  and the drop toward  $z \sim 0$ . When these processes are incorporated in the modeling of galaxy formation, they should recover the bi-modality features and solve other open puzzles.

*Subject headings:* cooling flows — dark matter — galaxies: evolution — galaxies: formation — galaxies: halos — shock waves

### 1. INTRODUCTION

Observations reveal a robust bi-modality in the galaxy population, being divided into two major classes at a characteristic stellar mass of  $M_{s,\text{crit}} \simeq 3 \times 10^{10} M_{\odot}$ . This corresponds to halos of mass  $M_{\text{crit}} \simeq 6 \times 10^{11} M_{\odot}$  and virial velocity  $V_{\text{crit}} \simeq 120 \text{ km s}^{-1}$  today. In a nut shell, less massive galaxies tend to be blue, star-forming disks residing in the “field”. Their properties are correlated along a “fundamental line” of decreasing surface brightness, internal velocity and metallicity with decreasing luminosity down to the smallest dwarf galaxies. Galaxies above the critical mass are dominated by spheroids of red, old stars, with high surface brightness and metallicity independent of luminosity. They tend to reside in the high-density environments of groups and clusters and they preferentially host Active Galactic Nuclei (AGN). The mean halo mass-to-light ratio has a minimum at the critical scale.

Current models of galaxy formation have difficulties in reproducing this bi-modality and the broad color distribution observed. In particular, at the bright-red end, already at  $z \sim 1$ , there is a population of extremely red and luminous galaxies which are not a natural outcome of the current models. These galaxies require efficient star formation at earlier epochs, followed by an effective shut-down of star formation in big galaxies. At the blue end, the observations reveal very blue galaxies in excess of the model predictions, indicating repeat-

ing episodes of bursty star formation over the lifetime of each galaxy. At low redshifts, the blue sequence is non-trivially truncated at the bright end, while at  $z \geq 2$ , there are indications for very luminous starbursts in big objects, both posing a severe challenge to the current models.

#### 1.1. *The observed bi-modality*

The bi-modality or transition in galaxy properties is observed in many different ways. We list here the main relevant observed features,<sup>1</sup> and address their origin below in §8.

(a) **Luminosity functions.** Blue galaxies dominate the stellar mass function below  $M_{s,\text{crit}}$ , while red galaxies take over above  $M_{s,\text{crit}}$  (Baldry et al. 2004; Bell et al. 2003b, in SDSS and 2MASS respectively). The transition scale corresponds to a luminosity slightly below the characteristic luminosity of the brightest disk galaxies,  $L_*$  of the Schechter function, beyond which the luminosity function drops exponentially.

(b) **Color-magnitude.** A color bi-modality shows robustly in color-magnitude diagrams, where the galaxies are divided into a blue sequence and a red sequence separated by a gap. In SDSS (Blanton et al. 2003; Baldry et al. 2004), the gap is at  $u-r \sim 2$ . The color distribution is non-trivially *broad*, with the red tip stretching beyond  $u-r = 2.5$  and the blue tail reaching well below  $u-r = 1.0$ .

(c) **Star-formation rate.** The current star-formation rate

(SFR), and the typical age of the stellar population, as measured by several different spectral indicators, show a robust bi-modality about  $M_{s,\text{crit}}$ . The less massive galaxies are dominated by young populations, while the more massive galaxies are dominated by old stars (Kauffmann et al. 2003; Madgwick et al. 2003, in SDSS and 2dF respectively), in agreement with the color bi-modality. A similar bimodality is seen in the gas-to-stellar mass fraction, which is high in the blue sequence and low in the red sequence, steeply increasing with stellar mass below  $M_{s,\text{crit}}$ , and only moderately so above it (Kannappan 2004, in SDSS+2MASS).

(d) **Color-magnitude at  $z \sim 1$ .** The color bi-modality is similar back to  $z \sim 1.5$  (Bell et al. 2004, in COMBO17). Extremely red massive galaxies (EROs) exist at the bright tip of the red sequence already at  $z \sim 1$  (e.g. Moustakas et al. 2004). Very blue small galaxies indicating starbursts show in the blue sequence (e.g. Ferguson & Babul 1998; Fioc & Rocca-Volmerange 1999).

(e) **Massive starbursts at high  $z$ .** Very luminous and massive dusty objects are detected at  $z \sim 2-4$ , indicating an excessive activity of star formation in surprisingly big objects (Shapley et al. 2004; Smail et al. 2002; Chapman et al. 2003, 2004, LBG and SCUBA sources).

(f) **Star-formation history.** The cosmological history of star-formation rate has a broad maximum near  $z \sim 1-2$ , followed by a sharp drop from  $z \sim 1$  to  $z = 0$  (e.g. Madau et al. 1996; Dickinson et al. 2003; Hartwick 2004; Giavalisco et al. 2004; Heavens et al. 2004). Still, about half the stars in today's spirals seem to have formed after  $z \sim 1$ , e.g. in luminous infrared galaxies (LIRGs) near  $M_{s,\text{crit}}$  (Hammer et al. 2004).

(g) **Bulge-to-disk ratio.** The galaxy bulge-to-disk ratio, as evaluated from the light concentration or the Sersic index, shows a transition near  $M_{s,\text{crit}}$  from disk domination at smaller masses to spheroid domination at larger masses (Kauffmann et al. 2003; Blanton et al. 2003, in SDSS). The red sequence seems to be dominated by spheroids, and the blue sequence by disks.

(h) **Environment dependence.** The distributions in color and SFR depend strongly on the galaxy density in the  $\sim 1\text{Mpc}$  vicinity: the young, blue (mainly disk) population is dominant in low-density environments, while the old, red (mostly spheroid) sequence is dominant in high-density environments (Hogg et al. 2003; Kauffmann et al. 2004; Blanton et al. 2003; Balogh et al. 2004; Blanton et al. 2004, in SDSS). The color-environment correlation is stronger than the well known morphology-density relation of Dressler (1980).

(i) **Halo mass and HOD.** The environment density is correlated with the mass of the host dark-matter halo, where halos less massive than  $\sim 10^{12}M_{\odot}$  typically host one dominant galaxy each while more massive halos tend to host groups and clusters of luminous galaxies, as quantified by the Halo Occupation Distribution (HOD, Yan et al. 2003; Abazajian et al. 2004; Kravtsov et al. 2004, in 2dF, SDSS and in simulations respectively). The environment dependence thus implies that the galaxy properties are primarily determined by the mass of the host halo (Blanton et al. 2004), and the bi-modality/transition in galaxy properties is associated with a characteristic dark-halo virial mass of  $M_{\text{crit}} \lesssim 10^{12}M_{\odot}$ .

(j) **Groups and hot halo gas.** Groups tend to be dominated by one type of galaxies, ellipticals *or* spirals (Hickson, Kindl & Huchra 1988). The spiral fraction is

anti-correlated with the group velocity dispersion  $\sigma_{\text{v}}$  and with the X-ray temperature and luminosity; the transition occurs near  $\sigma_{\text{v}} \sim 140\text{km}\text{s}^{-1}$  (Helsdon & Ponman 2003; Osmond & Ponman 2004). In particular, inter-galactic X-ray radiation is detected predominantly in groups where the brightest galaxy is an elliptical. For  $L_{\text{B}} < 10^{10.5}L_{\odot}$  elliptical galaxies the X-ray luminosity can be attributed to discrete sources, but brighter ellipticals typically show a significant excess of X-ray flux which is plausibly associated with hot halo gas (Ciotti et al. 1991; Mathews & Brighenti 2003).

(k) **Luminosity/mass functions.** The stellar-mass (or luminosity) function has a “knee” near  $M_{s,\text{crit}}$  ( $\lesssim L_{*}$ ), where the shallow  $dn/dM_s \propto M_s^{-1}$  of the faint side turns into an exponential drop. In contrast, the dark-halo mass function, as predicted in the standard  $\Lambda\text{CDM}$  model, is  $dn/dM \propto M^{-1.8}$  everywhere below  $\sim 10^{13}M_{\odot}$ . These two functions can be matched at  $M_{s,\text{crit}}$  if the baryonic fraction in galaxies is  $M_s/M \sim 0.05$ , indicating gas loss compared to the universal value  $\simeq 0.13$ , and again associating  $M_{s,\text{crit}} \simeq 3 \times 10^{10}M_{\odot}$  with  $M_{\text{crit}} \simeq 6 \times 10^{11}M_{\odot}$ . However, the function shapes are discrepant both at the faint and bright ends, posing challenges for theory. Correspondingly, the halo mass-to-light function has a minimum near  $M_{\text{crit}}$ , varying as  $M/L \propto M^{-2/3}$  and  $\propto M^{+1/2}$  below and above it respectively, thus implying increased suppression of star formation away from the critical mass on both sides (Marinoni & Hudson 2002; Bell, Baugh, Cole, Frenk & Lacey 2003; Bell, McIntosh, Katz & Weinberg 2003a; Yang, Mo & van den Bosch 2003, in a B-mag sample and in SDSS, 2MASS, 2dF respectively). Matching the luminosity function of central galaxies in halos to the CDM subhalo mass function indicates a similar transition near  $M_{\text{crit}}$  (Tasitsiomi et al. 2004, ; Wechsler & White, in preparation). Accordingly, the luminosity of brightest cluster galaxies, above  $M_{\text{crit}}$ , are growing very slowly with cluster halo mass (Lin & Mohr 2004).

(l) **Fundamental line vs. plane.** A transition is detected in the galaxy structural scaling relations near  $M_{s,\text{crit}}$ . The mean effective surface brightness (or, equivalently, the half-light radius) changes from  $\mu_s \propto M_s^{0.6}$  at lower masses to  $\mu_s \sim \text{const.}$  at the bright end (Kauffmann et al. 2003; Shen et al. 2003, in SDSS). The correlation below  $M_{s,\text{crit}}$  is part of the “fundamental line” relating the stellar mass to the radius and rotation velocity, which extends over five orders of magnitude in  $M_s$  down to the smallest dwarf galaxies in the Local Group (e.g. Dekel & Woo 2003). The mean metallicity as a function of stellar mass shows a similar transition near a similar scale, from  $Z \sim M_s^{0.4}$  at the low end to  $Z \sim \text{const.}$  at the high end (Tremonti et al. 2004; Dekel & Woo 2003, in SDSS and the Local Group respectively).

(m) **AGN.** Black hole masses are correlated with their host spheroid masses and dispersion velocities (e.g. Tremaine et al. 2002). The optical AGN population (e.g. based on  $O_{III}$ ), with high accretion rate and SFR, peaks near  $M_{s,\text{crit}}$  with little AGN activity at smaller masses, and is associated with black-hole masses  $\lesssim 10^8M_{\odot}$  (Kauffmann et al. 2003, in SDSS). Radio-loud AGNs, uncorrelated with the optical activity and the SFR, dominate in larger halos hosting  $\sim 10^{8-9}M_{\odot}$  black holes (G. Kauffmann, private communication).

## 1.2. Key Physical Processes

The bi-modality observed in so many different ways, with the robust characteristic scale imprinted on almost every global property of galaxies, cries for a theoretical understanding. We address three basic physical processes, show that they conspire to emphasize the same characteristic scale, and integrate them into a scenario which attempts to address simultaneously the variety of observed phenomena:

(a) **Cold flows versus hot medium.** The thermal history of the gas as it flows through the halo into the central disk is qualitatively different below and above a critical mass scale of  $\sim 10^{11-12} M_\odot$  (Birnboim & Dekel 2003; Keres et al. 2004). In less massive halos, the disk is built by cold flows ( $\sim 10^{4-5} \text{K}$ ), which are likely to generate early bursts of star formation. In more massive halos, the infalling gas is first heated by stable shocks to near the virial temperature ( $\sim 10^6 \text{K}$ ). Near and above the shock-heating scale at  $z \leq 2$  (and preferentially in relatively isolated galaxies), streams of dense cold gas penetrate through a dilute shock-heated medium (Fardal et al. 2001; Kravtsov 2003; Keres et al. 2004) (discussed in §2-§5).

(b) **Gravitational clustering.** Non-linear gravitational clustering of the large-scale dark-matter distribution is known to occur on a characteristic mass scale,  $M_*$ , corresponding to the typical halos forming at a given epoch and the lower bound for groups of galaxies. Its rapid growth in time is determined by the amplitude and shape of the initial fluctuations power spectrum and the background cosmology (§A). We point out that the clustering scale happens to roughly coincide with the shock-heating scale at  $z \sim 1$ , and the interplay between these two scales plays a major role in determining the galaxy properties (§5-§6).

(c) **Feedback processes.** We argue that the main feedback processes affecting galaxy evolution are all relatively ineffective near the critical shock-heating scale, partly due to the shock-heating process itself, and thus they help stressing the imprint of this scale on the galaxy properties. Supernova feedback is efficient in galaxies below the critical scale (Dekel & Silk 1986), where the potential wells are shallow enough for the energy fed to the interstellar medium after a burst of star formation to heat most of the gas, or even blow it away. Radiative feedback is also limited to halos below the shock-heating scale. These feedbacks regulate the star formation rate into episodic bursts and drive the fundamental line (Dekel & Woo 2003). Feedback by AGNs, or other sources such as dynamical friction in clusters and thermal instability into a two-phase medium, can become efficient in halos more massive than the shock-heating and clustering scale. They preferentially affect the dilute shock-heated medium and may prevent it from ever cooling and forming stars, while cold, dense clouds and streams are more likely to be shielded against these feedback effects (§7).

We show below how the introduction of shock-stability physics crystallizes our understanding of the origin of the characteristic scales of galaxies, and how it can be used to significantly improve the classical scenario of galaxy formation. We argue below that the combination of shock heating, feedback and clustering introduces a fundamentally new feature in galaxy-formation modeling — *a complete suppression of cold gas supply in halos above a critical mass after a critical redshift*. This could be the key to solving many of the main open questions in galaxy-formation theory, such as the bright-end truncation of the luminosity function, the appear-

ance of very red bright galaxies already at  $z \sim 1$ , and the indications for massive starbursts at higher redshifts. We note that some of the issues discussed in this paper, especially involving the cold versus hot gas modes and the role of feedback in explaining the bright-end of the luminosity function, have been addressed in a similar spirit and in different ways by Birnboim & Dekel (2003), Benson et al. (2003), Keres et al. (2004) and Binney (2004).

## 1.3. outline

In sections 2 to 7 we address the three physical processes and how they give rise to a similar characteristic scale. §2-5 address the shock-heating process in some detail, building upon the original analysis of Birnboim & Dekel (2003, hereafter BD03). In §2 we describe how the phenomenon is realized in simulations, in §3 we bring our analytic understanding of it, and in §4 we compute the associated critical mass scale in the cosmological context. Then, in §5, we address the phenomenon of cold streams in hot halos as seen in the cosmological simulations, and elude to the possible connection with the independent clustering scale. This brings us to §6, where we briefly discuss the role of this clustering scale in setting up the minimum mass for galaxy groups and thus relate it to the environment dependence of the bimodality. In §7, we address the various relevant feedback processes working below and above the critical scale, and point out their cross-talk with the shock heating process.

Following the presentation of these three physical processes, we integrate them in §8 into a scenario which attempts to explain the origin of the bi-modality and the associated observed features.

In the final three sections we discuss several implications and issues related to the broader perspective of galaxy formation. In §9 we address the role of shock heating and feedback in the formation of galaxies in small halos. In §10 we discuss the possible relevance to several other open issues in galaxy formation. In §11 we summarize our results, the proposed re-engineering of galaxy formation simulations, and the open issues.

## 2. SHOCK-HEATING SCALE: SIMULATIONS

The standard paradigm of disk formation (Rees & Ostriker 1977; Silk 1977; White & Rees 1978; Blumenthal, Faber, Primack & Rees 1984; White & Frenk 1991; Mo, Mao & White 1998), which lies at the basis of all current models of galaxy formation, assumes that while a dark-matter halo relaxes to a virial equilibrium, the gas that falls in within it is *shock heated* near the halo virial radius  $R_v$  to the halo virial temperature. It is then assumed to cool radiatively from the inside out. As long as the cooling time is shorter than a certain global free-fall time (or the Hubble time), typically inside a current “cooling radius”, the gas is assumed to accrete gradually onto a central disk and then form stars in a quiescent way. The maximum halo mass for efficient cooling was estimated to be on the order of  $\sim 10^{12-13} M_\odot$ , and the common wisdom has been since then that this explains the upper bound for disk galaxies. However, early hints, based on one-dimensional simulations, indicated that this scenario cannot reproduce the sharp drop in the luminosity function above this scale (Thoul & Weinberg 1995). Even earlier studies, valid in the context of the pancake picture of galaxy formation, indicated

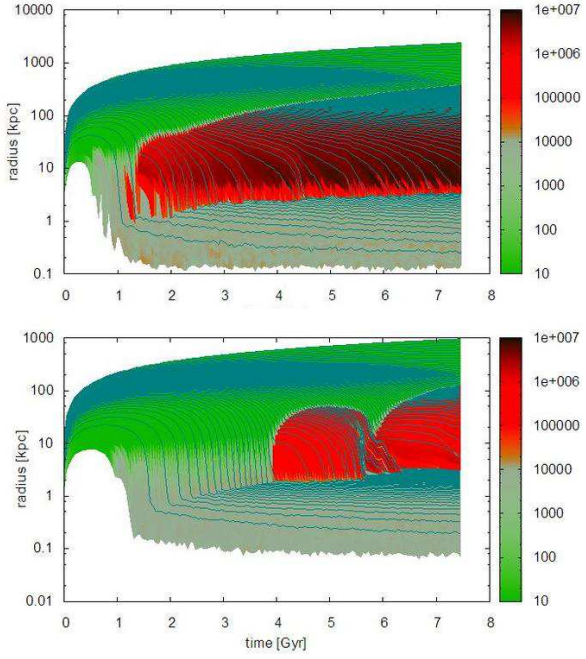


FIG. 1.— Time evolution of the radii of Lagrangian gas shells (lines) in a spherical simulation of a protogalaxy consisting of primordial gas ( $Z = 0$ ) and dark matter. Temperature is marked by color. A shock shows up as a sharp break in the flow lines, namely a sudden slowdown of the infall, associated with an abrupt increase in the temperature. The lower discontinuity where the inflow is brought to a final halt marks the “disk” radius, formed due to an artificial centrifugal force. (a) A massive system, where the virialized mass grows from  $10^{11}$  to  $10^{13} M_{\odot}$ . (b) A less massive system, growing from  $10^{10}$  to  $10^{12} M_{\odot}$ . A virial shock exists only in systems more massive than a critical mass, while in smaller halos the gas flows cold and unperturbed directly into the disk. With more realistic metallicities the critical mass becomes  $\sim 10^{12} M_{\odot}$ .

that virial shock heating may not be as general as assumed (Binney 1977). More advanced cosmological simulations have started to reveal the presence of cold flows (Fardal et al. 2001). With the new data from big surveys such as SDSS, 2MASS and 2dF, and the detailed semi-analytic modeling (SAM) of galaxy formation, it is becoming clear that the observed scale is somewhat smaller and the drop is sharper than predicted by the original picture. It seems that the current models based on the standard paradigm have hard time trying to reproduce many of the observed bi-modality features summarized in §1. This motivated us to attempt a closer look at the shock-heating mechanism.

### 2.1. Spherical simulations

Fig. 1 shows the time evolution of the radii of Lagrangian gas shells in a spherical gravitating system consisting of gas (in this case with primordial composition) and dark matter, simulated by BD03 using an accurate one-dimensional hydrodynamical code. Not shown are the dissipationless dark-matter shells, which detach from the cosmological expansion, collapse and oscillate into virial equilibrium such that they deepen the potential well attracting the dissipating gas shells. The initial density perturbation was assumed to have a profile proportional to the linear two-point correlation function of  $\Lambda$ CDM (justified in Dekel 1981), and the final density profile roughly mimics the universal NFW profile derived from cosmological simulations. The gas is cooling radiatively based on the atomic cooling function computed by

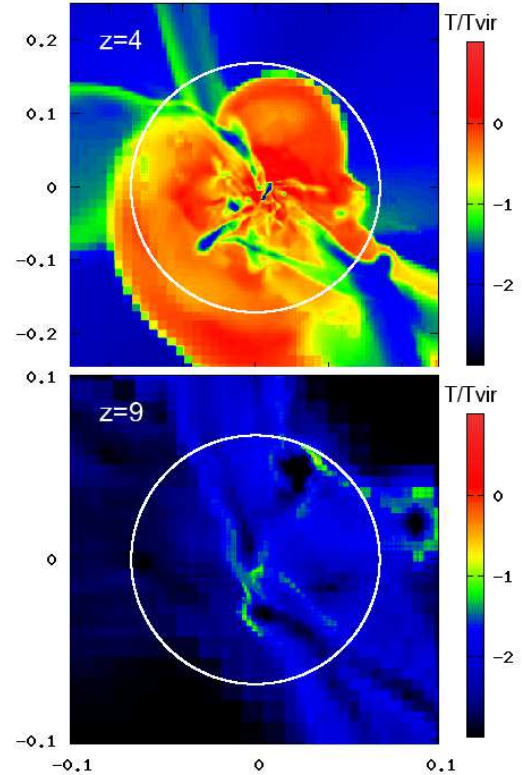


FIG. 2.— Snapshots from a cosmological hydrodynamical simulation (courtesy of Andrey Kravtsov), showing the gas temperature in a slice of a protogalaxy at two different epochs, when it has two different masses. The temperature is relative to the virial temperature of the halo at that time. The side of each slice is scaled to be  $3R_v$ , with the numbers in comoving  $h^{-1}$  Mpc. **Top:** At  $z \simeq 4$ , when the halo is already relatively massive,  $M \simeq 3 \times 10^{11} M_{\odot}$ . Much of the gas is heated by a strong shock near the virial radius (marked by a circle). Cold streams penetrate through the hot medium deep into the halo toward the central disk. **Bottom:** At  $z \simeq 9$ , when the halo is still rather small,  $M \simeq 2 \times 10^{10} M_{\odot}$ . The gas flows in cold ( $T \ll T_v$ ), showing no evidence for shock heating inside the virial radius (circle).

Sutherland & Dopita (1993). The collapse of each gas shell is stopped at roughly  $0.05R_v$  by an artificial centrifugal force which mimics the formation of a central disk. The upper panel focuses on massive halos of  $\sim 10^{12} M_{\odot}$ . As expected in the common picture, a strong shock exists near the virial radius, namely at roughly half the maximum-expansion radius of the corresponding shell. The virial shock gradually propagates outward, encompassing more mass in time. The hot post-shock gas is in a quasi-static equilibrium, pressure supported against gravitational collapse. The lower panel focuses on halo masses smaller by an order of magnitude, and shows an interesting new phenomenon. A stable shock forms and inflates from the disk toward the virial radius only after a total mass of more than a few times  $10^{11} M_{\odot}$  has collapsed. In less massive systems, the cooling rate is faster than the compression rate required for restoring the pressure in the post-shock gas; had there been a shock, the post-shock gas would have become unstable against gravitational contraction and unable to support the shock. In the specific case shown, with zero metallicity, the critical mass is biased low; with more realistic metallicities it becomes  $\sim 10^{12} M_{\odot}$  due to the additional cooling by metal lines (§4).

### 2.2. Cosmological simulations

Results from cosmological hydro simulations indicate that the phenomenon is not restricted to spherical systems. They

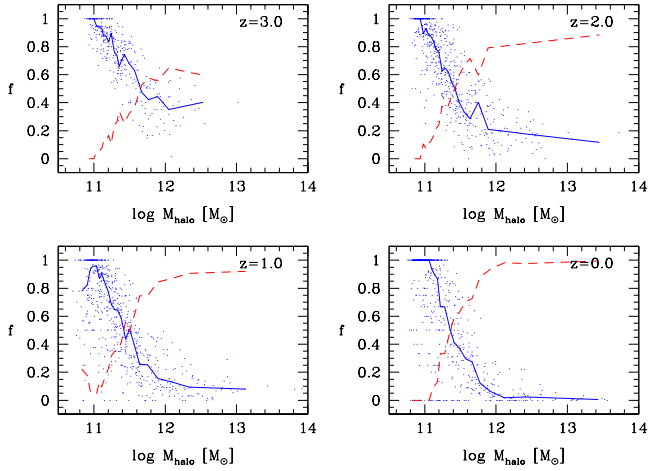


FIG. 3.— The cold accretion fraction as a function of halo mass at  $z = 3, 2, 1$ , and  $0$  in the SPH simulation of Keres et al. (2004, figure 6). Points show the cold fractions of individual galaxies, and solid lines show the median values in bins of halo mass. Dashed lines show the median hot fraction; the solid and dashed curves sum to one by definition. (courtesy of Dusan Keres et al.)

indicate further that our stability criterion discussed below may in fact be approximately valid in the general case where the inflow is predominantly along filaments. Fig. 2 displays snapshots from Eulerian simulations by A. Kravtsov (unpublished pictures; the simulations were described and used for other purposes in Kravtsov 2003; Kravtsov & Gnedin 2004), showing the gas temperature in two epochs in the evolution of a protogalaxy: one at  $z \simeq 4$ , when the halo is already relative massive,  $M \simeq 3 \times 10^{11} M_\odot$ , and the other at  $z \simeq 9$ , when the halo is still rather small,  $M \simeq 2 \times 10^{10} M_\odot$ . While the more massive halo, near the critical scale, shows a hot gas component near the virial temperature behind a virial shock, the smaller halo shows only cold flows inside the virial radius.

Similar results have been obtained earlier from SPH simulations by Fardal et al. (2001), who emphasized the feeding of galaxies by cold flows preferentially at early epochs. We now understand that this redshift dependence mostly reflects the smaller masses of halos at higher redshifts. Keres et al. (2004) have analyzed similar SPH simulations and presented the case for the two modes of infall, cold and hot, in more detail.<sup>2</sup> For example, in their figures 1 and 2 they demonstrate the two-mode phenomenon very convincingly by showing the distribution of particles and their trajectories in temperature-density diagrams. Figure 3, borrowed from Keres et al. (2004, figure 6), shows the fractions of cold and hot infall as a function of halo mass at different redshifts. One can see that for all halos of masses below a critical mass the infall is predominantly cold. Near the critical mass there is a relatively sharp transition into a hot mode, which becomes dominant above the critical mass. The transition from 100% cold to more than 50% hot occurs across a factor of only  $\sim 2$  in halo mass. In this simulation, where zero metallicity is assumed, the transition mass is  $M \sim 3 \times 10^{11} M_\odot$  at all redshifts in the range  $0-3$ .

The spherical simulations described above, and the analytic analysis described below (§3, §4), yield very similar results. In fact, our predictions for the case of zero metallicity match

<sup>2</sup> The hot phase becomes an “infall” mode in this simulation after the gas cools, but in reality it may be kept hot and be prevented from falling in by feedback effects, §7.

the critical mass measured by Keres et al. (2004) remarkably well.

Note in Fig. 3 that the cold mode does not always vanish above the shock-heating mass; in many galaxies it exists simultaneously with the hot mode, especially at high redshifts and in relatively isolated galaxies. The massive halo in Fig. 2 demonstrates that this coexistence is typically in the form of filamentary cold streams penetrating through the rather spherical hot medium toward the central disk. The cold mode may also contain compact clumps, possibly associated with the cold flows. We return to this phenomenon in §5.

### 3. SHOCK-STABILITY ANALYSIS

#### 3.1. Post-shock stability criterion

The behavior seen in the simulations is understood via a straightforward stability analysis of the post-shock gas, first introduced in BD03. We provide here a brief, improved presentation of this analysis, followed by a more detailed estimate of the predicted critical mass for shock stability as a function of redshift.

A stable extended shock can exist when the pressure in the post-shock gas is sufficient to balance the gravitational attraction toward the halo center. The standard equation of state for an ideal gas expresses the pressure as  $P = (\gamma - 1)\rho e$  where  $\rho$  and  $e$  are the gas density and internal energy per unit mass, and  $\gamma = 5/3$  for a mono-atomic gas. In the textbook case of no cooling, the adiabatic index is defined as  $\gamma \equiv (\partial \ln P / \partial \ln \rho)_{\text{ad}}$ , and the system is known to be gravitationally stable once  $\gamma > 4/3$ . When there is energy loss (e.g. by radiation) at a rate  $q$  per unit mass, we define a new quantity along the particle trajectories:

$$\gamma_{\text{eff}} \equiv \frac{d \ln P}{d \ln \rho} = \gamma - \frac{\rho}{\dot{\rho}} \frac{q}{e}. \quad (1)$$

The second equality follows from energy conservation,  $\dot{e} = -P\dot{V} - q$  (where  $V = 1/\rho$ ), plugged into the equation of state. Note that  $\gamma_{\text{eff}} = \gamma$  when  $q = 0$ . The difference between the two is a ratio of characteristic rates for the two competing processes: the cooling, which reduces the pressure in the post-shock gas, and the compression due to the pattern of the post-shock infall, which tends to increase the pressure. If the compression rate is efficient compared to the cooling-loss rate, it restores the pressure necessary for supporting a stable extended shock, but otherwise the post-shock gas collapses inward under gravity, failing to support the extended shock.

It is convenient to express the *compression rate* in the post-shock region as the inverse of a compression time, which we define by

$$t_{\text{comp}} \equiv \Gamma \frac{\rho}{\dot{\rho}}, \quad \Gamma \equiv \frac{3\gamma+2}{\gamma(3\gamma-4)} = \frac{21}{5}, \quad (2)$$

with the factor  $\Gamma$  to be justified below, and the last equality referring to  $\gamma = 5/3$ . For a spherical shock at radius  $r_s$ , and a post-shock radial velocity  $u_1$ , we assume that the radial flow pattern in the post-shock region is homologous,  $u/r = u_1/r_s$ . This is justified based on the spherical simulations described above, where the log-linear post-shock flow lines in Fig. 1 are nearly parallel straight lines. We then obtain using continuity

$$t_{\text{comp}} = \frac{\Gamma}{(-\nabla \cdot \mathbf{u})} = \frac{\Gamma r_s}{(-3u_1)}. \quad (3)$$

The competing *cooling rate* in the post-shock region is expressed as the inverse of the standard radiative cooling time defined by

$$t_{\text{cool}} \equiv \frac{e}{q}, \quad (4)$$

where  $e = e(T)$  and  $q \propto \rho \Lambda(T, Z)$ , functions of temperature  $T$  and metallicity  $Z$ . Then in eq. (1)

$$\gamma_{\text{eff}} = \gamma - \Gamma^{-1} \frac{t_{\text{comp}}}{t_{\text{cool}}}. \quad (5)$$

In order to test for stability, BD03 performed a perturbation analysis where the radius of a shell is perturbed by  $r \rightarrow r + \delta r$  and the sign of the force,  $\delta \ddot{r} / \delta r$ , is computed. Writing  $\delta r = u \delta t$ , using the homology, and assuming further that the gravity and pressure forces balance each other near the transition state between stability and instability,  $\rho^{-1} \nabla P = GM/r^2$ , one obtains a restoring force, i.e. stability, for

$$\gamma_{\text{eff}} > \gamma_{\text{crit}} \equiv \frac{2\gamma}{\gamma+2/3} = \frac{10}{7}. \quad (6)$$

The  $\gamma_{\text{crit}} = 10/7$  replaces the standard  $\gamma_{\text{crit}} = 4/3$  of the adiabatic case.<sup>3</sup>

Using eq. (5) and the definitions of the time scales above, the *shock stability criterion* of eq. (6) becomes the simple condition that *the cooling rate should be slower than the compression rate*:

$$t_{\text{cool}} > t_{\text{comp}}. \quad (7)$$

Once the cooling rate is slower, the pressure gain by compression can balance the loss by radiative cooling, which allows the post-shock gas to be stable against global gravitational collapse and thus support the shock. The factor  $\Gamma = 21/5$  has been introduced in the definition of  $t_{\text{comp}}$ , eq. (2), in order to simplify this final expression.

Note that the relevant quantity for stability is the *ratio* of rates associated with the two competing processes, independent of how slow each of them actually is in absolute terms. Each of the characteristic times could in principle be longer than the Hubble time – it is their ratio which determines whether a stable shock is possible or the gas falls in subject to gravity, cold and unperturbed.

### 3.2. Pre-shock quantities

#### 3.2.1. Compression rate

Using the standard jump conditions across a strong shock, we can express the characteristic time scales (or  $\gamma_{\text{eff}}$ ) in terms of the pre-shock gas quantities. The jump condition for the radial velocity is

$$u_0 - u_s = \frac{\gamma+1}{\gamma-1} (u_1 - u_s), \quad (8)$$

where  $u_s$  is the radial shock velocity and  $u_0$  is the radial velocity of the pre-shock gas. Then

$$t_{\text{comp}} = \frac{\Gamma(\gamma+1)}{3(\gamma-1)} \frac{r_s}{|u_0|} \left( 1 - \frac{2}{(\gamma-1)} \frac{u_s}{|u_0|} \right)^{-1} \quad (9)$$

<sup>3</sup> If the spherical symmetry assumed above is replaced by planar symmetry, both for the shock and the gravitational field, the stability criterion  $\gamma_{\text{eff}} > 10/7$  is replaced by  $\gamma_{\text{eff}} > 10/11$  (Birnboim, Dekel & Kravtsov, in preparation). One can therefore assume in general that the actual critical value lies somewhere between these two limits; if  $\gamma_{\text{eff}} < 10/11$  there is no stable shock, if  $\gamma_{\text{eff}} > 10/7$  the conditions allow a stable shock, and if  $10/11 < \gamma_{\text{eff}} < 10/7$  the shock stability depends on the local geometry.

$$= \frac{28}{5} \frac{r_s}{|u_0|} (1 - 3\tilde{u}_s)^{-1} \quad (10)$$

$$\simeq 5.48 \text{Gyr} \frac{r_s}{|u_0|} (1 - 3\tilde{u}_s)^{-1}, \quad (11)$$

where  $\tilde{u}_s \equiv u_s/|u_0|$  (see §3.2.4) and the last expression assumes  $\gamma = 5/3$ ,  $r_s$  in 100 kpc, and  $u_0$  in 100 km s<sup>-1</sup>. If  $u_s = 0$ , say, then  $t_{\text{comp}}$  is about 6 times larger than  $r_s/|u_0|$ , a typical free-fall time from  $r_s$  into the halo center. At the virial radius,  $t_{\text{comp}}$  is comparable to the Hubble time at the corresponding epoch, but at inner radii it becomes significantly shorter.

#### 3.2.2. Cooling rate

The cooling time (e.g. based on Sutherland & Dopita 1993) is

$$t_{\text{cool}} \equiv \frac{e}{q} = \frac{(1+2\epsilon)}{(1+\epsilon)} \frac{3}{2} kT \left[ \frac{\chi^2}{m} \rho \Lambda(T, Z) \right]^{-1}, \quad (12)$$

where  $\Lambda(T, Z)$  is the cooling function,  $k$  is the Boltzmann constant,  $\epsilon \equiv n_{\text{He}}/n_H$ , the mass per particle is  $m \equiv \mu m_p$  with  $\mu = (1+4\epsilon)/(2+3\epsilon)$ , and the number of electrons per particle is  $\chi = (1+2\epsilon)/(2+3\epsilon)$ . For 25% He in mass, one has  $\epsilon = 1/12$ , yielding  $\mu = 0.59$ . If we express the post-shock temperature as  $T_6 \equiv T/10^6 \text{K}$ , the post-shock baryon density as  $\rho_{-28} \equiv \rho/10^{-28} \text{g cm}^{-3}$ , and the cooling function as  $\Lambda_{-22}(T, Z) \equiv \Lambda(T, Z)/10^{-22} \text{erg cm}^3 \text{s}^{-1}$ , we have

$$t_{\text{cool}} \simeq 2.61 \text{Gyr} \rho_{-28}^{-1} T_6 \Lambda_{-22}^{-1}(T, Z). \quad (13)$$

The post-shock gas density is related to the pre-shock density by the jump condition

$$\rho_1 = \frac{\gamma+1}{\gamma-1} \rho_0 = 4\rho_0, \quad (14)$$

and the post-shock temperature entering the cooling time is related to the pre-shock radial velocity  $u_0$  via

$$\frac{kT_1}{m} = \frac{2(\gamma-1)}{(\gamma+1)^2} (u_0 - u_s)^2 = \frac{3}{16} u_0^2 (1 + \tilde{u}_s)^2. \quad (15)$$

We note in passing that for a virial shock, where  $u_0 = -V_v$  (BD03), the post-shock temperature is actually

$$T_1 \gtrsim \frac{3}{8} T_v, \quad (16)$$

comparable to but somewhat smaller than the virial temperature as defined in eq. (A9).

#### 3.2.3. Stability criterion

Using eqs. 11 and 13, the critical stability condition becomes

$$\frac{t_{\text{cool}}}{t_{\text{comp}}} \simeq 0.48 \frac{\rho_{-28}^{-1} T_6 \Lambda_{-22}^{-1}(T, Z)}{r_s |u_0|^{-1} (1 - 3\tilde{u}_s)^{-1}} \simeq 1, \quad (17)$$

with  $r_s$  in 100 kpc and  $u_0$  in 100 km s<sup>-1</sup>. Recall that eq. (14) relates  $\rho$  to  $\rho_0$ , and eq. (15) relates  $T$  to  $u_0$ . Thus, for given shock radius  $r_s$ , shock velocity relative to infall  $u_s/|u_0|$ , and pre-shock gas density  $\rho_0$ , once the metallicity  $Z$  is given and the cooling function  $\Lambda(T, Z)$  is known, one can solve eq. (17) for the critical values of  $T$  and the corresponding  $u_0$ . When put in a cosmological context (§4), this solution is associated with a unique critical halo mass.

The stability criterion derived above, eq. (6) or eq. (7), is found to work very well when compared to the results of the

spherical simulations of BD03. When  $\gamma_{\text{eff}}$  (or  $t_{\text{cool}}/t_{\text{comp}}$ ) is computed using pre-shock quantities at a position just outside the “disk”, we find that as long as the halo is less massive than a critical scale, before the shock forms, the value of  $\gamma_{\text{eff}}$  is indeed well below  $\gamma_{\text{crit}}$  and is gradually rising, reaching  $\gamma_{\text{crit}}$  almost exactly when the shock starts propagating outward. The value of the  $\gamma_{\text{eff}}$  computed using the quantities just outside the shock then oscillates about  $\gamma_{\text{crit}}$  with a decreasing amplitude, following the oscillations in the shock radius seen in Fig. 1. As the shock eventually settles at the virial radius,  $\gamma_{\text{eff}}$  approaches  $5/3$ , larger than  $\gamma_{\text{crit}} = 10/7$ , where the cooling is negligible.

The same analytic stability criterion is found to be valid also in three-dimensional hydrodynamical cosmological simulations, where it has been used to identify the cold streams without explicit information concerning the presence or absence of the actual shocks (Birnboim, Dekel & Kravtsov, in preparation). When testing the criterion in these simulations, in which the hot phase and the cold phase may be present simultaneously, the local gas properties at each position are first transformed to post-shock quantities, as if there was a shock there, and the stability is evaluated based on the derived value of  $\gamma_{\text{eff}}$  there. The resultant maps of  $\gamma_{\text{eff}}$  resemble quite well the temperature maps of the actual simulation. This demonstrates that the wisdom gained by the spherical analysis is also applicable in the general case.

### 3.2.4. Shock velocity

What value of  $\tilde{u}_s$  is relevant for evaluating stability? In the inner halo, we use  $\tilde{u}_s = 0$ . This is because, as the halo is growing in mass, the shock first forms in the inner halo and then propagates outward (Fig. 1b). The onset of shock stability is therefore marked by its ability to develop a velocity outward.

During the stable phase when the shock is expanding with the virial radius, the spherical simulations indicate roughly  $u_1 \simeq -\tilde{u}_s$  (Fig. 1a), namely  $\tilde{u}_s \simeq 1/7$  (eq. 8). This indicates that a small shock velocity of such a magnitude is appropriate for evaluating stability at the virial radius.

Note that stability is harder to achieve when the shock is expanding relatively fast. In particular, in the extreme case  $\tilde{u}_s = 1/3$ , the post-shock velocity vanishes,  $u_1 = 0$  (eq. 8). The compression rate becomes infinitely slow (eq. 3), implying that the shock cannot be stabilized.

## 4. SHOCK-HEATING SCALE IN COSMOLOGY

### 4.1. Halos in cosmology

We wish to translate the critical stability condition, eq. (7) or eq. (17), into a critical post-shock temperature, and the corresponding critical halo virial velocity and mass as a function of redshift. Eq. (17) has a unique solution when combined with the two virial relations between halo mass, velocity and radius (eq. A6), and the relation between post-shock temperature and pre-shock infall velocity (eq. 15).

As summarized in Appendix A, the time dependence of the virial relations can be expressed in terms of the convenient parameter

$$A \equiv (\Delta_{200} \Omega_{m0.3} h_{0.7}^2)^{-1/3} a, \quad (18)$$

where  $a \equiv 1/(1+z)$  is the cosmological expansion factor and the other parameters are of order unity. The parameters  $\Omega_{m0.3}$  and  $h_{0.7}$  correspond to today’s values of the cosmological

mass density parameter and the Hubble expansion parameter respectively, and for the standard  $\Lambda$ CDM cosmology adopted here they are both equal to unity. The parameter  $\Delta_{200}$  is the virial density factor given approximately in eq. (A8): at redshifts  $z > 1$  it is  $\Delta_{200} \simeq 1$ , but at lower redshifts it becomes somewhat larger, reaching  $\Delta_{200} \simeq 1.7$  at  $z = 0$ .

### 4.2. Compression rate

For a shock at the virial radius,  $r_s = R_v$ , we approximate  $u_0 = -V_v$ , as predicted by the spherical collapse model in an Einstein-deSitter cosmology (BD03, Appendix B).

When the shock is at an arbitrary inner radius  $r$ , where the infall velocity is  $|u|$ , we multiply  $R_v$  and  $V_v$  by appropriate factors  $f_r \equiv r/R_v$  and  $f_u \equiv |u|/V_v$  (discussed in §4.5). Then eq. (11) becomes

$$t_{\text{comp}} \simeq 14.3 \text{Gyr} A^{3/2} f_r f_u^{-1} (1 - 3\tilde{u}_s)^{-1}. \quad (19)$$

### 4.3. Cooling rate: gas density

In order to express the cooling time of eq. (13) in terms of cosmological quantities, we first evaluate the pre-shock baryon density, which we write as

$$\rho_b = 4 f_b (\rho/\bar{\rho})_{\text{vir}} \Delta \rho_u f_\rho. \quad (20)$$

Here  $\rho_u$  is the universal mean mass density (eq. A4), and  $\Delta$  is the top-hat mean overdensity inside the virial radius (eq. A8). The factor  $(\rho/\bar{\rho})_{\text{vir}}$  translates  $\bar{\rho}$ , the mean total density interior to  $R_v$ , to  $\rho$ , the local total density at  $R_v$ . The effective baryonic fraction  $f_b$  turns it into a pre-shock baryonic density. The factor 4 stands for the ratio between the post-shock gas density and the pre-shock gas density.<sup>4</sup> The factor  $f_\rho \equiv \rho(r)/\rho(R_v)$  reflects the ratio of the actual gas density at some radius  $r$  within the halo to its value at the virial radius (see §4.5).

The ratio  $\rho/\bar{\rho}$  at the virial radius is derived for the universal NFW halo density profile revealed by cosmological simulations (Navarro, Frenk & White 1997). For a virial concentration parameter  $c$ , this ratio is

$$\left(\frac{\rho}{\bar{\rho}}\right)_{\text{vir}} = \frac{c^2}{3(1+c)^2} \left[ \ln(1+c) - \frac{c}{(1+c)} \right]^{-1}. \quad (21)$$

A typical concentration of  $c = 12$  is associated with  $\rho/\bar{\rho} \simeq 0.17$ ; we therefore express the approximate results below using the factor  $f_{\bar{\rho},0.17} \equiv (\rho/\bar{\rho})/0.17$ . In our more accurate evaluation of the critical scale (§4.7), we model the dependence of the mean concentration on mass and time using the fit of Bullock et al. (2001) for the  $\Lambda$ CDM cosmology:

$$c(M, a) = 18 M_{11}^{-0.13} a. \quad (22)$$

The effective baryon fraction  $f_b$  may in principle be as large as the universal fraction  $\simeq 0.13$ , but it is likely to be smaller because of gas loss due to outflows. For the approximate expressions we define  $f_{b,0.05} \equiv f_b/0.05$ .

The gas density at  $r$ , eq. (20), thus becomes

$$\rho_{-28} = 0.190 A^{-3} f_{b,0.05} f_\rho f_{\bar{\rho},0.17}. \quad (23)$$

Inserting this baryon density into eq. (13), the cooling time becomes

$$t_{\text{cool}} = 13.7 \text{Gyr} A^3 f_{b,0.05} f_\rho f_{\bar{\rho},0.17}^{-1} f_{T,0.17}^{-1} T_6 \Lambda_{-22}^{-1}(T, Z). \quad (24)$$

<sup>4</sup> In the spherical simulations, the relevant factor relating the baryon density to the dark matter density in eq. (20) is actually closer to  $\sim 3$  because of a “bump” in the dark-matter density just inside the virial radius.

The cooling function that we use below (based on Sutherland & Dopita 1993) neglects two physical processes: Compton scattering off the cosmic microwave background and the possible effect of external radiation on the cooling rate through the reionization of Hydrogen. Based on the more complete cooling function as implemented by Kravtsov & Gnedin (2004), one learns that these processes become important only for densities below  $\sim 10^{-28}$  and  $\sim 10^{-26}$  g cm $^{-3}$  at  $z \sim 0$  and 4 respectively. Using eq. (23), we conclude that while these processes may have a certain effect on the cooling rate near the virial radius, they should be negligible once the analysis is applied inside the inner half of the halo, where the critical scale for shock heating is determined in practice. We address these effects in more detail elsewhere (Birnboim, Dekel & Loeb, in preparation).

#### 4.4. Metallicity

The metallicity near the virial radius and in the inner halo, which also enters the cooling rate, is one of our most uncertain inputs. For the mean metallicity  $Z$  (in solar units) as a function of redshift  $z$  we use the two-parameter functional form

$$\log(Z/Z_0) = -sz, \quad (25)$$

where  $Z_0$  is today's metallicity and the slope  $s$  governs the rate of growth.

An upper limit may be imposed by the hot, X-ray emitting Intra-Cluster Medium (ICM) at low redshifts, which indicate  $Z_0 \sim 0.2 - 0.3$ . The ICM metallicity evolution in Semi-Analytic Models, assuming a range of different feedback recipes, yields consistently an average enrichment rate of roughly  $s \simeq 0.17$  (R. Somerville, private communication; De Lucia, Kauffmann & White 2004). We adopt this enrichment rate  $s$  in our modeling below.

A realistic estimate of the metallicity near the virial radius (or perhaps a lower limit for the inner halo) may be provided by  $C_{IV}$  absorbers in the Inter-Galactic Medium (IGM) at  $z \sim 2 - 4$  (Schaye et al. 2003). At densities appropriate to typical NFW halos at  $z = 3$  (with  $c = 3$ ), namely  $\rho_{\text{vir}} \simeq 53\rho_{\text{u}}$ , they measure an average of  $[C/H] = -2.47$ . Silicon measurements, on the other hand, seem to indicate a metallicity that is about five times larger (A. Aguirre, private communication). If one takes the geometrical mean between the metallicities indicated by  $C_{IV}$  and by Si one has  $Z(z = 3) \simeq 0.0075$ . This translates to  $Z_0 = 0.025$  if  $s = 0.17$ .

We note that another popular indicator,  $\text{Mg}_{II}$ , indicates consistently  $Z < 0.01$  within  $50 - 100$  kpc of galaxy centers at  $z \sim 1$  (private communication with J. Charlton; e.g. Ding et al. 2003).

The Damped Lyman-Alpha Systems (DLAS) are believed to sample cold gas deeper inside the halos, and can thus provide another interesting limit. Observations in the range  $z = 1 - 4$  (Prochaska et al. 2003) can be fitted on average by eq. (25) with  $Z_0 \simeq 0.2$  and a somewhat steeper slope  $s \simeq 0.26$ . However, a fit with  $s = 0.17$  (and then  $Z_0 = 0.1$ ) is not ruled out.

Based on the above estimates, we adopt as our fiducial metallicities  $Z_0 = 0.03$  at  $R_v$  and  $Z_0 = 0.1$  at the "disk" radius  $\sim 0.1R_v$ , both with an enrichment rate  $s = 0.17$ .

#### 4.5. Inside the halo

For a shock in the inner halo we wish to estimate the factors  $f_r$ ,  $f_u$  and  $f_\rho$ .

Empirically from the spherical simulation of BD03, for a shell encompassing a mass just shy of the critical mass (as well as from the toy model of BD03 of gas contracting in a static isothermal sphere), we estimate for  $f_r \equiv r/R_v$

$$f_\rho = \frac{\rho_0(r)}{\rho_0(R_v)} \simeq \begin{cases} f_r^{-1.6}, & r \lesssim R_v \\ f_r^{-2.1}, & r \sim 0.1R_v \end{cases}. \quad (26)$$

We adopt below  $f_\rho = f_r^{-2}$  at  $f_r = 0.1$ .

Energy conservation assuming pure radial motion inside a static singular isothermal sphere yields

$$f_u \equiv \frac{u_0(r)}{u_0(R_v)} = [1 + 2f_b(f_r^{-1} - 1) + 2(1 - f_b)\ln f_r^{-1}]^{1/2}. \quad (27)$$

For  $f_r = 0.1$  and  $f_b = 0.05$  this gives the estimate  $f_u \simeq 2.5$ .

Based on the definition of  $f_u$ , the temperature behind a virial shock is related to the temperature obtained from the stability condition at radius  $r$  by

$$T(R_v) = f_u^{-2} T(r). \quad (28)$$

#### 4.6. Crude explicit estimates

The critical temperature for stability, as obtained by comparing  $t_{\text{cool}}$  and  $t_{\text{comp}}$  in the cosmological context, eq. (24) and eq. (19), is

$$T_6 \lambda_{-22}^{-1}(T, Z) = 1.04 A^{-3/2} F, \quad (29)$$

where

$$F \equiv f_r f_u^{-1} f_\rho f_{b,0.05} f_{\tilde{u},0.17} (1 - 3\tilde{u}_s)^{-1}. \quad (30)$$

The cooling function as computed by Sutherland & Dopita (1993) can be crudely approximated in the range  $0.1 < T_6 < 10$  by

$$\Lambda_{-22} \simeq 0.12 Z_{0.03}^{0.7} T_6^{-1} + 0.02 T_6^{1/2}, \quad (31)$$

where  $Z_{0.03} \equiv Z/0.03$ , with  $Z$  in solar units. The above expression is valid for  $-2.5 \leq \log Z \leq 0$ , and at lower metallicities the value of  $\Lambda$  is practically the same as for  $\log Z = -2.5$ . This fit is good near  $T_6 \sim 1$  for all values of  $Z$ . The first term refers to atomic cooling, while the second term is due to Bremsstrahlung. For an approximation relevant in halos near the critical shock-heating scale we ignore the Bremsstrahlung term, which becomes noticeable only at higher temperatures. One can then obtain in eq. (29) an analytic estimate for the critical temperature:

$$T_6 \simeq 0.36 A^{-3/4} (Z_{0.03}^{0.7} F)^{1/2}. \quad (32)$$

Using eq. (15) and eq. (28), with  $|u_0| = V_v$  just outside the virial radius, we then obtain for the critical velocity and mass

$$V_{100} \simeq 1.62 A^{-3/8} (Z_{0.03}^{0.7} F)^{1/4} f_u^{-1} (1 + \tilde{u}_s)^{-1}, \quad (33)$$

$$M_{11} \simeq 25.9 A^{3/8} (Z_{0.03}^{0.7} F)^{3/4} f_u^{-3} (1 + \tilde{u}_s)^{-3}. \quad (34)$$

A comment regarding the  $\tilde{u}_s$  dependence of our results. The critical temperature depends on the shock velocity  $\tilde{u}_s$  via  $F$ ,  $T \propto (1 - 3\tilde{u}_s)^{-1/2}$ , reflecting the  $\tilde{u}_s$  dependence of  $t_{\text{comp}}$ . The critical temperature is thus monotonically increasing with  $\tilde{u}_s$ . An additional  $\tilde{u}_s$  dependence enters when the temperature is translated to a critical virial velocity using the jump condition,  $V \propto (1 + \tilde{u}_s)^{-1} T^{1/2}$ , and then to a critical mass,  $M \propto (1 + \tilde{u}_s)^{-3} T^{3/2}$ . For a slowly moving shock,  $\tilde{u}_s \ll 1/3$ , the combined  $\tilde{u}_s$  dependence of the critical mass is  $M \propto [1 + (9/4)\tilde{u}_s](1 - 3\tilde{u}_s) \simeq 1 - (3/4)\tilde{u}_s$  — a decreasing

function of  $\tilde{u}_s$ . This means that at a given radius in a halo of a given mass, when everything else is equal, a slowly expanding shock is actually more stable than a shock at rest. For example, if the shock is expanding with  $\tilde{u}_s = 1/7$  rather than  $\tilde{u}_s = 0$ , the critical mass is smaller by about 24%. However, recall that stability is harder to achieve when the shock is expanding relatively fast, and the compression completely vanishes if  $\tilde{u}_s \geq 1/3$  (§3.2.4).

For actual crude estimates of the critical scales at  $z = 0$ , we assume  $f_{b,0.05} \simeq f_{\rho,0.17} \simeq 1$ . For a shock at the *virial radius*,  $r = f_u = f_\rho = 1$ , we assume  $Z_0 \simeq 0.03$  and  $\tilde{u}_s \simeq 1/7$ , and obtain

$$T_6 \simeq 0.5, \quad V_{100} \simeq 1.6, \quad M_{11} \simeq 26. \quad (35)$$

At an *inner radius* closer to the disk vicinity, say  $f_r = 0.1$ , we estimate  $f_u \simeq 2.5$  and  $f_\rho \simeq 100$  (§4.5). Assuming  $Z_0 \simeq 0.1$  and  $\tilde{u}_s \simeq 0$ , we obtain

$$T_6 \simeq 1.1, \quad V_{100} \simeq 1.1, \quad M_{11} \simeq 8.8. \quad (36)$$

We see that for a shock at  $r \sim 0.1R_v$ , the expected critical mass is smaller than at  $R_v$ , somewhat below  $\sim 10^{12}M_\odot$ .

The above estimates are useful for exploring the qualitative dependences of the critical values on redshift, metallicity and gas fraction. For example, in eq. (34), the explicit redshift dependence and the decrease of metallicity with redshift tend to lower the critical mass toward higher  $z$ . On the other hand, the decrease of halo concentration with  $z$  (i.e. increase of  $f_{\rho,0.17}$ ), and the possible increase of the effective gas fraction with  $z$  (§8), tend to push the critical mass up at higher  $z$ .

#### 4.7. More accurate estimates

We now obtain a better estimate of the critical temperature (and then critical mass and virial velocity) by solving eq. (29) using the exact cooling function of SD93 and adopting specific models for the time evolution of metallicity and halo structure. The results are presented graphically.

The baryon density is computed assuming an NFW profile whose concentration evolves in time as in eq. (22). The effective fraction of cold gas is assumed to be  $f_b = 0.05$ , motivated by best fits of semi-analytic models to the Milky Way (Klypin, Zhao & Somerville 2002) and by fitting the  $\Lambda$ CDM halo mass function to the observed luminosity function near  $L_*$  (Bell et al. 2003). The metallicity evolution is parametrized as in eq. (25) with  $s = 0.17$  for today's metallicities in the range  $Z_0 = 0.03 - 0.3$ . Upper and lower estimates for the critical scales are evaluated at the virial radius and at  $r = 0.1R_v$  respectively, using the crude estimates of §4.5. In the following figures the shock is assumed to be at rest,  $u_s = 0$ .

Figure 4 shows the critical mass as a function of redshift. At a typical inner-halo radius,  $r = 0.1R_v$ , we plot the curves for three different current metallicities:  $Z_0 = 0.03, 0.1, 0.3$ . The critical halo mass, for  $Z_0 = 0.1$ , is  $\simeq 6 \times 10^{11}M_\odot$  quite independent of redshift. The uncertain metallicity introduces a scatter by a factor of 2 up and down (for  $z < 2.5$ ).

An upper limit of  $\sim 2 \times 10^{12}M_\odot$  is obtained for a shock at  $R_v$  when a correspondingly low metallicity is assumed,  $Z_0 = 0.03$ . When the assumption of  $\tilde{u}_s \simeq 0$  is replaced by  $\tilde{u}_s \simeq 1/7$ , allowing the shock to expand with the virial radius as seen in Fig. 1a, the critical mass at  $R_v$  with  $Z_0 = 0.03$  becomes comparable to that at  $0.1R_v$  with  $Z_0 = 0.3$ .

Figure 5 shows the corresponding virial velocity. At  $z = 0$  the critical virial velocity for a shock in the inner halo is

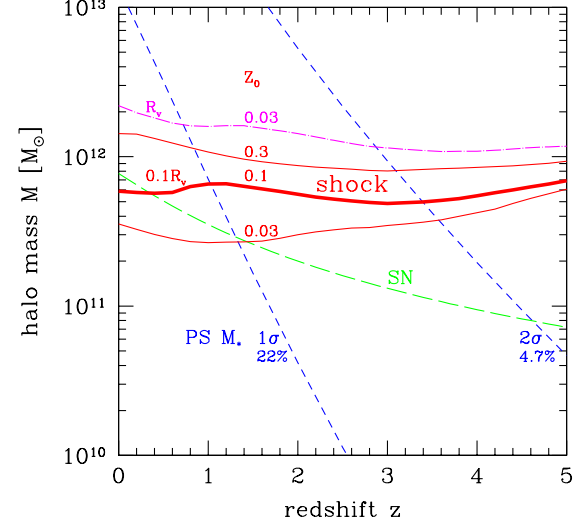


FIG. 4.— Critical shock-heating halo mass as a function of redshift. The three solid (red) curves refer to a shock at the inner halo,  $r = 0.1R_v$ , with different metallicities as indicated; the middle curve ( $Z_0 = 0.1$ ) is our best estimate. The dash-dotted (magenta) curve refers to a shock at the virial radius with  $Z_0 = 0.03$ . The other parameters used are:  $f_b = 0.05$ ,  $u_s = 0$ ,  $s = 0.17$  (see text). Shown for comparison (short dash, blue) are the Press-Schechter estimates of the forming halo masses, corresponding to  $1-\sigma$  ( $M_*$ ) and  $2-\sigma$ , where the fractions of total mass in more massive halos are 22% and 4.7% respectively. Also shown is the critical mass for supernova feedback discussed in §7.1 (long dash, green).

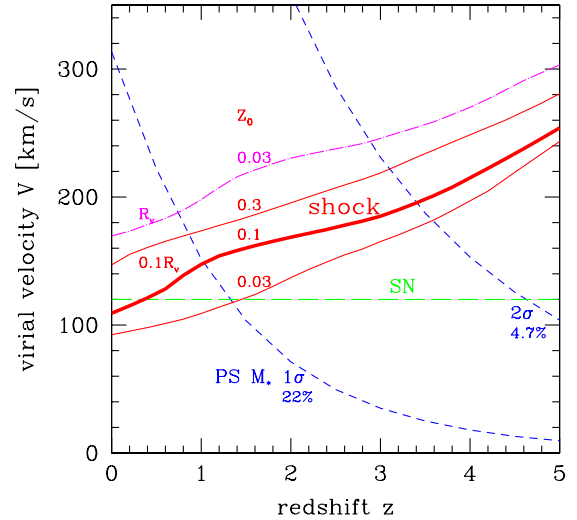


FIG. 5.— Same as Fig. 4 but for the corresponding halo virial velocity.

$\sim 120 \text{ km s}^{-1}$ , with a  $\pm 30 \text{ km s}^{-1}$  scatter due to metallicity. The critical virial velocity increases monotonically with redshift, to  $\sim 200 \text{ km s}^{-1}$  near  $z \sim 3$  (a crude fit to the redshift dependence is  $V_v = 120 + 28z$ ).

The dependence on metallicity at  $z = 0$  is highlighted in Fig. 6. The metallicity enters strongly through the cooling function  $\Lambda(T, Z)$ . The critical mass grows roughly like  $Z^{1/2}$ , as predicted in eq. (34), so it spans about an order of magnitude over the whole metallicity range.

The analytic estimates of eq. (33) and eq. (34), based on the approximate cooling function, turn out to provide good estimates in most cases, and can therefore be used for extending the results analytically to any desired choice of the relevant

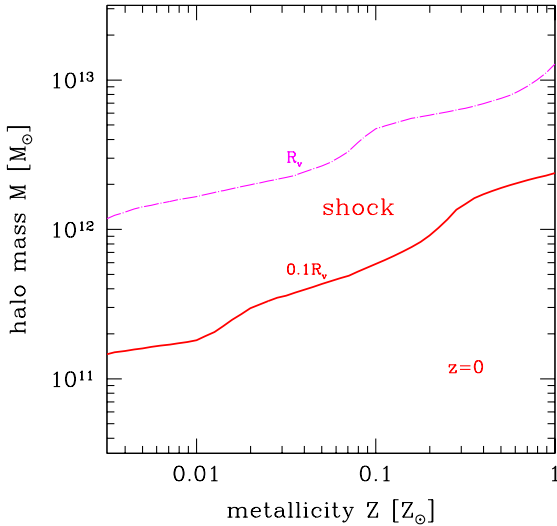


FIG. 6.— Critical shock-heating halo mass as a function of metallicity at redshift  $z = 0$ . The solid (red) curve refers to a shock at the inner halo,  $r = 0.1 R_v$ . The dash-dotted (magenta) curve refers to a shock at the virial radius.

parameters.

We learn that the critical halo mass for shock stability at the disk vicinity,  $M_{\text{shock}}(r_{\text{disk}})$ , is somewhat smaller than for a shock at the virial radius,  $M_{\text{shock}}(R_v)$ . This result is robust: it is true even if the metallicity at the virial radius is smaller by an order of magnitude than the metallicity at the disk, and even when  $\bar{u}_s$  at  $R_v$  is as large as 1/7. This means that as the halo is growing in mass, the conditions for a stable shock develop first in the inner halo and somewhat later in the outer halo. Thus, in halos of mass  $M < M_{\text{shock}}(r_{\text{disk}})$ , we expect cold flows with no shock heating throughout the halo. In the other extreme of halos of mass  $M > M_{\text{shock}}(R_v)$ , we expect shock heating of most of the gas by a shock near the virial radius. In halos of mass in the narrow intermediate range  $M_{\text{shock}}(r_{\text{disk}}) < M < M_{\text{shock}}(R_v)$ , we expect shock heating somewhere inside the halo, preventing the gas from falling in and giving rise to a hot medium. Note that this predicted mass range is consistent with the range of transition from all cold to mostly hot seen in the cosmological simulations, Fig. 3, i.e. a factor of 2-3 in mass. We discuss below (§5) the appearance of cold streams along the denser filaments in halos in this regime.

Also shown in Fig. 4 are the typical masses of halos forming at different redshifts, the 1- $\sigma$  (termed  $M_*$ ) and 2- $\sigma$  halo masses according to the Press-Schechter formalism, eq. (A18). According to the improved Sheth-Tormen version, the corresponding fractions of the total mass encompassed in halos exceeding the mass  $M$  are 22% and 4.7% respectively. One can see in Fig. 4 that the critical scale for shock heating coincides with  $M_*$  at  $z \sim 1$ , and with the 2- $\sigma$  mass at  $z \sim 3.4$ . By  $z \sim 2$ , say, most of the forming halos are significantly less massive than the shock-heating mass. When embedded in a large-scale high- $\sigma$  density peak, the distribution of forming halos at a given  $z$  may shift toward more massive halos. In fact, the most massive halo in a volume of comoving size  $\sim 100 \text{ Mpc}$  is likely to be more massive than  $10^{12} M_\odot$  at all relevant redshifts ( $z < 6$ , say). Nevertheless, the qualitative result concerning the majority of the halos remains valid. We conclude that *in the vast majority of forming galaxies the gas has never been shock-heated to the virial temperature* — it rather flows *cold* all the way to the disk vicinity.

We note that the values obtained for the shock-heating scale at low redshifts are compatible with the observed bimodality/transition scale summarized in §1. The estimates in the inner halo, using the lower and upper limits for  $Z_0$ , indeed border the observed characteristic halo mass of  $\sim 6 \times 10^{11} M_\odot$ . The upper-limit estimate at  $R_v$  corresponds to a halo mass similar to that of the Milky Way.

## 5. COLD STREAMS IN A HOT MEDIUM

### 5.1. In the simulations

As seen in the simulation of Kravtsov shown in Fig. 2, massive halos at high redshift show cold streams embedded in a hot medium. This is supported by the analysis of Keres et al. (2004) shown in Fig. 3, demonstrating that the cold mode may in some cases coexist with the hot mode even above the shock-heating scale, especially at  $z > 2$ . We wish to understand the origin of this phenomenon, and learn about its dependence on cosmological time.

The simulation results of Keres et al. (2004) provide several additional clues. First, they show in their figures 17 and 18 that the cold infall tends to be *filamentary*, especially at high redshifts, while the hot mode is more spherical. They report that the directional signal measuring filamentary infall in the cold accretion mode is stronger for halos above the shock-heating scale while the cold accretion is more isotropic in lower mass halos.

Second, they show in figure 16 that the cold accretion is on average of *higher density* than the hot mode. This is by only a factor of two or so (perhaps underestimated because they mix small and large halos in this analysis), but since the shock is responsible for a density increase by a factor of 4, the actual difference between the hypothetical post-shock (or pre-shock) densities is more like a factor of 8. Similarly, Nagai & Kravtsov (2003) find in their simulation of a massive halo that the filamentary structure is associated with gas entropy ( $\propto T/\rho^{2/3}$ ) *far below* that of the surrounding halo gas, consistent with a shorter cooling time in the filaments.

Third, Keres et al. (2004) display in their figure 13 the *environment* dependence of the gas infall modes, showing that the cold and hot modes dominate at low and high neighborhood densities respectively. As a function of redshift, one learns that at  $z < 2$  the cold mode dominates for galaxy densities below  $n_{\text{gal}} \sim 0.3 (h^{-1} \text{Mpc})^{-3}$  and becomes negligible at larger environment densities, while at  $z = 3$  the cold mode is more pronounced than the hot mode for all neighborhood densities up to  $n_{\text{gal}} \sim 10 (h^{-1} \text{Mpc})^{-3}$ . The environment density is correlated with the mass of the host halo (§6), so the variation with redshift of the environment dependence could be partly attributed to the finding of a significant cold mode in massive halos at high  $z$  (Fig. 3). However, the environment dependence may also partly reflect variations in the HOD at a given halo mass.

### 5.2. Interplay with the clustering scale

Our understanding of the appearance of cold streams in massive halos is along the following lines. As noted already, in addition to the shock-heating scale there is another, independent and very important characteristic scale in the problem — the scale of *nonlinear clustering*,  $M_*$ , corresponding to the typical mass of halos forming at a given epoch. The cosmological model determines the perturbation growth rate,

and then the initial fluctuation power spectrum, its shape and especially its normalization amplitude, determines the actual clustering scale. The masses for  $1\sigma$  halos ( $M_*$ ) and for  $2\sigma$  halos, based on eq. (A18) with  $\nu = 1$  and 2 respectively, are shown again in Fig. 7.

As far as the dark matter is concerned, one expects the large-scale structure to be roughly self-similar in time when masses are measured in terms of  $M_*$  and densities in terms of the background universal density.<sup>5</sup> We learn from cosmological N-body simulations (including Keres et al. 2004) that this is indeed the case for the large-scale filamentary structure: the characteristic width of the filaments is comparable to  $R_*$ , the size of an  $M_*$  halo, while the typical filament length is larger by about an order of magnitude and scales similarly in time. While the  $M \gg M_*$  halos are typically at the nodes of intersecting filaments which are typically thin compared to the halo size, many of the  $M \sim M_*$  halos are actually embedded in such filaments and thus see a wide-angle infall pattern. Assuming that at any given epoch the accretion rate of dark matter,  $\dot{M}$ , is proportional to the halo mass  $M$ , while the virial densities in halos of all masses are the same, this geometrical difference implies that the densities in the filaments penetrating  $M \gg M_*$  halos are higher by a factor of a few than the typical densities in their host halos. On the other hand, the densities in the filaments that build  $M \sim M_*$  halos are comparable to the typical halo densities.

Assuming that the density of the gas flowing along the filaments scales with the dark-matter density, and that the infall velocity is comparable to the halo virial velocity, we conclude that the cooling time in the filaments should be shorter by a factor of a few than in the surrounding spherical halo. If the compression time in the filaments is comparable to that in the host halo, this implies that the thin filaments have a harder time supporting a stable shock. Therefore, the critical halo mass for shock heating in the filaments feeding it must be larger than the estimate for a spherical virial shock (§4).

A crude way to evaluate the maximum halo mass for cold streams at a given redshift may be as follows. Recall that the critical ratio for shock stability (eq. 17) scales roughly like

$$\frac{t_{\text{cool}}}{t_{\text{comp}}} \propto \frac{\rho^{-1} T \Lambda^{-1}}{R V^{-1}}, \quad (37)$$

with  $T$ ,  $R$  and  $V$  the halo virial quantities and  $\rho$  the gas density. At a given epoch, the typical halo  $\rho$  and  $R/V$  are roughly independent of halo mass (based on the definition of the virial radius), so with the virial relation  $T \propto M^{2/3}$ , and approximating the cooling function with  $\Lambda \propto T^{-1}$  (eq. 31), the critical ratio for spherical infall in halos is

$$\left( \frac{t_{\text{cool}}}{t_{\text{comp}}} \right)_{\text{halo}} = \left( \frac{M}{M_{\text{shock}}} \right)^{4/3}. \quad (38)$$

For a halo of mass  $M$ , assuming that  $R V^{-1}$  in the streams is the same as in their host halo, the critical ratio in the streams is inversely proportional to the density enhancement in the filaments compared to their host halo (eq. 37). If the streams' characteristic width is  $\propto (f M_*)^{1/3}$  compared to the halo size

<sup>5</sup> This would have been a perfect self-similarity had the cosmology been Einstein-deSitter and the power spectrum been a power law. However, the structure is close to being self-similar for the  $\Lambda$ CDM cosmology as well due to the fact that the deviations from self-similarity in the cosmology and the power spectrum are absorbed in the definition of  $M_*$ .

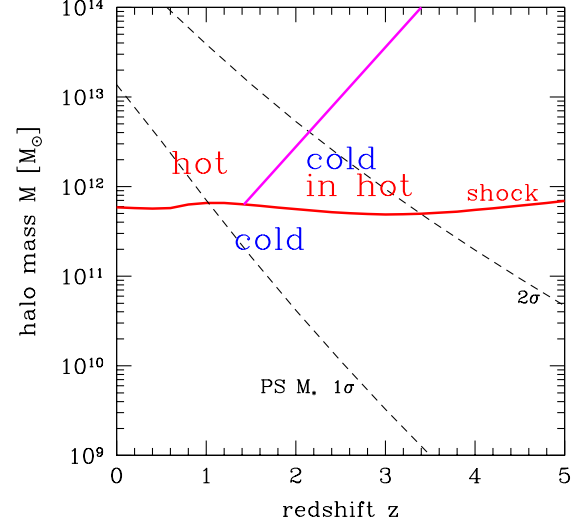


FIG. 7.— Cold streams and shock-heated medium as a function of halo mass and redshift. The nearly horizontal curve is the typical threshold mass for a stable shock in the spherical infall from Fig. 4, below which the flows are predominantly cold and above which a shock-heated medium is present. The inclined solid curve is the upper limit for cold streams from eq. (40) with an arbitrary choice of  $f = 3$ ; this upper limit is valid at redshifts higher than  $z_{\text{crit}} \sim 1-2$ , defined by  $M_{\text{shock}} > f M_*$ . The hot medium in  $M > M_{\text{shock}}$  halos at  $z > z_{\text{crit}}$  hosts cold streams which allow disk growth and star formation, while halos of a similar mass at  $z < z_{\text{crit}}$  are all hot, shutting off gas supply and star formation.

$\propto M^{1/3}$  (with  $f$  a factor of order a few), the density in the streams feeding a halo of mass  $M$  is higher than the halo density by the geometrical factor  $(f M_*/M)^{-2/3}$ . With eq. (38) one obtains

$$\left( \frac{t_{\text{cool}}}{t_{\text{comp}}} \right)_{\text{stream}} = \left( \frac{f M_*}{M} \right)^{2/3} \left( \frac{M}{M_{\text{shock}}} \right)^{4/3}. \quad (39)$$

For this ratio to equal unity in the streams, the critical halo mass is

$$M_{\text{stream}} \sim \frac{M_{\text{shock}}}{f M_*} M_{\text{shock}}, \quad f M_* < M_{\text{shock}}. \quad (40)$$

At low  $z$ , where  $f M_* > M_{\text{shock}}$ , cold streams exist only for  $M < M_{\text{shock}}$ . At high  $z$ , where  $f M_* < M_{\text{shock}}$ , cold streams appear even in  $M > M_{\text{shock}}$  halos where shocks heat part of the gas, as long as  $M < M_{\text{stream}}$ . The critical redshift  $z_{\text{crit}}$  separating these two regimes is defined by

$$f M_*(z_{\text{crit}}) = M_{\text{shock}}. \quad (41)$$

This maximum mass for cold streams is shown in Figure 7 for an arbitrary choice of  $f = 3$ .

This scenario is qualitatively consistent with the simulation results described in §2; the shock-heating mass explains the transition from cold to hot at a given mass roughly independent of  $z$ , and the presence of cold streams above  $M_{\text{shock}}$  at  $z > z_{\text{crit}}$  explains the dependence of the cold mode on redshift and environment. An additional part of the environment effect may be due to the survivability of cold streams in different environments; while they could survive unperturbed in relatively isolated galaxies, they may be harassed by the active intergalactic environment in dense groups. The properties of cold flows in halos as a function of halo mass, redshift, and grouping, which we have attempted to evaluate in a qualitative way, deserve a more quantitative analysis using high-resolution cosmological hydro simulations.

## 6. GROUP SCALE: COOLING & HOD

The multiplicity of galaxies in a group, and hence the environment density of galaxies, is a strong monotonic function of the host-halo mass. Since many of the galaxy properties are observed to be strong functions of the environment density, the minimum group mass scale at  $\sim 10^{12-13} M_\odot$  is obviously an important characteristic scale to be considered, and its cross-talk with the shock-heating scale should be addressed.

The distinction between halos hosting a single dominant galaxy and halos hosting groups of luminous galaxies has traditionally been attributed to the ability or inability of the gas in these halos to cool on a dynamical time scale (Rees & Ostriker 1977). The new finding that cold flows dominate the gas infall below a similar critical scale while the gas in more massive halos is shock heated lends further support to the original idea that the gas cooling process has an important role in determining the minimum group scale. The gas in a halo above the shock-heating mass cannot cool and collapse on a dynamical time scale into one dominant central galaxy. Instead, it can cool and collapse dynamically into several local fragments, each of a mass below the cooling or shock-heating scale.

However, with the advance of cosmological N-body simulations, it has become apparent that the independent gravitational dark-matter clustering process has a parallel important role in driving the group scale. Given the accretion history determined by the standard  $\Lambda$ CDM cosmology and the amplitude of initial fluctuations, combined with the processes of tidal stripping and dynamical friction during the nonlinear stages of group assembly, the halo occupation distribution develops a transition from single to multiple occupancy by subhalos near a comparable host-halo mass scale (Kravtsov et al. 2004); this HOD of simulated subhalos has a shape and a transition scale compatible with the HOD deduced from the observed correlation function for luminous galaxies in groups (§1, item *i*). Therefore, in halos above  $\sim 10^{12} M_\odot$ , the potential wells associated with the DM subhalo population provide ideal conditions for the fragmented gas collapse on the scale preferred by cooling, thus emphasizing this scale as the minimum scale for groups.

The gravitational origin of the group scale can be understood in simple terms. According to Press-Schechter theory, at time  $t$ , halos of masses  $M \sim M_*(t)$  are in the process of rapid growth by accreting satellites of all masses (smaller than  $M$ ); they make multiple-occupancy groups with relatively massive subhalos. On the other hand, halos of masses  $M \ll M_*(t)$ , those that managed not to have merged with bigger halos by time  $t$ , did most of their growth in the past when  $M_*(t)$  was comparable to  $M$  — they have not been accreting many more satellites after that epoch. Part of this effect can be attributed to the high cosmological velocity dispersion (comparable to the virial velocity of  $M_*$  halos) of small halos near the turnaround radius of a  $M \ll M_*$  halo, making them unlikely candidates for becoming bound satellites of such a small halo. In such halos, that were mostly built early, the big satellites with masses  $m \sim 0.01M$  and up (see below) have spiraled in by dynamical friction while being stripped by tides. Such halos therefore tend to host a dominant central galaxy with relatively small satellites, namely a “field galaxy” rather than a “group”.

In order to estimate the effect of dynamical friction on

the subhalo population, we use Chandrasekhar’s formula (Binney & Tremaine 1987; Zhao 2004) to approximate the time for a satellite of mass  $m$  to spiral from the virial radius into the center of an isothermal halo of mass  $M$  as

$$t_{\text{DF}}^{-1} \sim 2\pi G \rho \frac{Gm}{V_v^3} \ln \Lambda, \quad (42)$$

where  $\rho$  is the typical density in the outer halo,  $V_v$  is the halo virial velocity, the satellite velocity is assumed to be comparable to  $V_v$ , and  $\ln \Lambda$  is the Coulomb logarithm which is typically between unity and ten. Assuming that  $\rho$  is roughly 200 times the universal mean density at the time of halo formation  $t$ , we obtain

$$\frac{t}{t_{\text{DF}}} \sim (10-100) \frac{m}{M}. \quad (43)$$

If the satellites entered the halo at  $t \ll t_0$ , the dynamical friction has been working for a Hubble time,  $t_{\text{DF}} \sim t_0$ , and  $m$  can be interpreted as the most massive surviving satellite at  $t_0$ . For the standard  $\Lambda$ CDM cosmology, the typical forming halo in the  $z$  range  $[0, 1]$  is roughly  $M_* \simeq M_{*0} (t/t_0)^{3.5}$ , where  $M_{*0} \simeq 1.4 \times 10^{13} M_\odot$  (§A), so

$$\frac{m_{\text{max}}}{M} \sim (0.01-0.1) \left( \frac{M}{M_{*0}} \right)^{0.3}. \quad (44)$$

An indication for a similar trend of  $m_{\text{max}}$  with  $M$  is seen in N-body simulations (Gao et al. 2004). Thus, for halos significantly smaller than  $M_{*0}$ , that have stopped accreting satellites long ago, the most massive surviving satellite is of order 1% of the halo mass, not qualifying as a “group”. The threshold for halos hosting groups of subhalos is therefore somewhat below  $M_{*0}$ .

This group scale as predicted by gravity alone happens, by coincidence, to be comparable to the shock-heating (or cooling) scale at  $z \leq 1$ . The gravitational and cooling processes conspire to stress the minimum halo mass for groups. As argued below (§8), the coincidence of these two scales is likely to play an important role in the origin of the observed features, and especially their environment dependence. The clustering scale may also affect some of the feedback processes discussed below (e.g. §7.6). The possible interplay between the clustering scale and the appearance of cold filaments in hot halos has been addressed above (§5). In addition, given that this scale is also associated with grouping, the active environment in high-HOD halos may be expected to damage the cold-flow pattern and thus disable further disk growth and star formation.

## 7. FEEDBACK PROCESSES

Several different feedback processes are known to be playing an important role in the evolution of galaxies. Some are related to the shock-heating scale or the clustering scale, and others may be independent. We briefly address here some of the relevant processes, pointing to the fact that they tend to have a minimum effectiveness in halos of mass that is comparable to, or somewhat below the shock-heating and clustering scales. This amplifies certain observed features, such as the knee in the galaxy luminosity function associated with the minimum in  $M/L$  near the critical mass, and the maximum SFR at  $z \sim 1-2$ .

### 7.1. Supernova feedback

The process of supernova feedback is different from the shock-heating process, but it also yields a characteristic scale in the same ballpark (Dekel & Silk 1986). This may be partly a coincidence, because the initial supernova energy arises from stellar nuclear sources that have little to do with the galactic cooling and dynamical processes. However, there are possible connections through the involvement of similar cooling processes (and given that some aspects of the asymptotic behavior of a supernova remnant is not strongly dependent on its initial energy).

The energy fed to the inter-stellar gas by supernovae can be written as

$$E_{\text{SN}} \simeq \nu \epsilon \dot{M}_{\text{s}} t_{\text{rad}} \propto M_{\text{s}} (t_{\text{rad}}/t_{\text{dyn}}), \quad (45)$$

where  $\nu$  is the number of supernovae per unit mass of forming stars,  $\epsilon$  is the typical supernova energy, and  $t_{\text{rad}}$  is the time available for the supernova remnant to share its energy with the medium during its adiabatic phase, before a significant fraction of it is radiated away. This energy has been evaluated by DS86 based on the physics of expanding supernova remnants. The second proportionality follows from the crude assumption of a star-formation burst over a characteristic dynamical time,  $\dot{M}_{\text{s}} \sim M_{\text{s}}/t_{\text{dyn}}$ . DS86 pointed out that for halos in the relevant halo mass range, where the virial temperature is  $T \sim 10^5 \text{ K}$ , the cooling function behaves roughly like  $\Lambda \propto T^{-1}$  (eq. 31), and then  $t_{\text{rad}}/t_{\text{dyn}} \simeq 0.01$  — a constant for all galaxies. This implies the key nontrivial result that the energy fed to the gas is proportional to the stellar mass,  $E_{\text{SN}} \propto M_{\text{s}}$ , despite the significant radiative losses. When this energy input is compared to the energy required for significantly heating the gas or blowing it away,  $E_{\text{binding}} \simeq M_{\text{gas}} V^2$ , one ends up with the maximum virial velocity for effective supernova feedback,

$$V_{\text{SN}} \simeq 120 \text{ km s}^{-1}. \quad (46)$$

This critical velocity is pretty robust; it is very weakly dependent on the gas fraction, density and metallicity (e.g., DS86, eq. 49), and is therefore quite insensitive to redshift.

In halos which correspond to potential wells shallower than that implied by the critical velocity, the supernova feedback from a burst of stars with a standard initial mass function can significantly suppress further star formation, at least for a while, and thus regulate the star formation process. This can lead to low surface-brightness and dwarf galaxies, possibly with repeating episodes of star formation (§1, item *d*).

The observed correlations between the properties of galaxies below stellar mass of  $3 \times 10^{10} M_{\odot}$  lend support to the important role of supernova feedback on these scales. These correlations define a “fundamental line” (Dekel & Woo 2003), which stretches across five decades in luminosity down to the smallest dwarfs. The mean scaling relations, involving  $M_{\text{s}}$ , the velocity  $V$ ,<sup>6</sup> the surface brightness  $\mu$  (or alternatively the radius) and the metallicity  $Z$ , are approximately (Kauffmann et al. 2003; Tremonti et al. 2004; Dekel & Woo 2003)

$$V \propto M_{\text{s}}^{0.2}, \quad Z \propto M_{\text{s}}^{0.4}, \quad \mu \propto M_{\text{s}}^{0.6}. \quad (47)$$

This is to be compared to the familiar Tully-Fisher relation for brighter galaxies (Courteau et al. 2004),  $V \propto M_{\text{s}}^{0.3}$ , and the

lack of systematic dependence of  $Z$  and  $\mu$  on  $M_{\text{s}}$  there. Supernova feedback can explain the origin of the fundamental line in simple terms (Dekel & Woo 2003). The above energy criterion,  $E_{\text{SN}} \propto M_{\text{s}} \propto M_{\text{gas}} V^2$ , with the assumption that the relevant initial gas mass is a constant fraction of the halo mass,  $M_{\text{gas}} \propto M$ , immediately implies the relation driving the fundamental line:

$$M_{\text{s}}/M \propto V^2. \quad (48)$$

We then use the basic relation between the halo virial quantities,  $M \propto V^3 \propto R^3$  (eq. A6). For the metallicity we adopt the simplest approximation of instantaneous recycling,  $Z \propto M_{\text{s}}/M_{\text{gas}}$ . For the stellar radius we rely on the standard assumption of angular-momentum conservation (Fall & Efstathiou 1980; Mo, Mao & White 1998),  $R_* \propto \lambda R$ , with  $\lambda$  a constant spin parameter, and use it in the expression for surface brightness,  $\mu \propto M_{\text{s}}/R_*^2$ . Combining the relations from eq. (48) and on, we recover the scaling relations, eq. (47). The success of this simplest possible toy model is beyond the expectations given the crude approximations involved, but it indicates that supernova feedback could indeed be the primary driver of the fundamental line below the bimodality scale, which strengthens the association of this process with the origin of the transition scale itself (in concert with the shock heating discussed above, see §8).

Figure 5 shows the critical virial velocity for supernova feedback,  $V_{\text{SN}} = 120 \text{ km s}^{-1}$ , and Figure 4 shows how the corresponding halo mass is varying with redshift:  $M_{\text{SN}} \sim 7 \times 10^{11} M_{\odot}$  at  $z=0$ , decreasing to  $\sim 1.3 \times 10^{11} M_{\odot}$  at  $z=3$ . With an effective baryonic fraction of  $f_b \sim 0.05$ , the corresponding stellar mass at  $z=0$  is  $\sim 3.5 \times 10^{10} M_{\odot}$ , also practically coinciding with the observed bi-modality or transition scale.

### 7.2. UV-on-dust feedback

An additional feedback mechanism that may help regulating the star formation in a similar range of halo masses below the shock-heating scale has been proposed by Murray, Quataert & Thompson (2004). It is based on momentum-driven winds due to radiation pressure produced by the continuum absorption and scattering of UV photons from starbursts (or AGNs) on dust grains. While the dust grains cannot survive long enough in a hot medium of  $\sim 10^6 \text{ K}$  and above, they may provide a sufficient optical depth if the gas is cold and dense. Then, momentum deposition from star formation can expel a significant fraction of the cold gas once the luminosity is above a certain Eddington-like threshold obeying a Faber-Jackson type relation:  $L_{\text{max}} \propto f_b \sigma^4$ . A starburst that attains this maximum luminosity moderates its star formation rate and its luminosity does not increase further. Ellipticals and Lyman-Break Galaxies indeed seem to lie near and below the predicted  $L_{\text{max}}(\sigma)$  line.

We notice that the threshold mass for shock heating discussed above imposes an upper threshold for the operation of this feedback mechanism. Above the shock-heating scale, the dust grains are destroyed in the hot medium, and the fact that AGNs can replace the starbursts as the UV source cannot help.

Below the shock-heating scale, the presence of cold flows makes a difference in two ways: it provides much of the starbursts emitting the required UV flux and enriching the gas with metals, and it allows the survival of dust grains in high-column-density streams, thus creating an appropriate optical depth. This feedback is effective when the radiation bulk pressure overcomes the gas ram pressure. The ratio of these com-

<sup>6</sup> The velocity is taken to be the larger between the rotation velocity and  $\sqrt{2}\sigma$ , where  $\sigma$  is the dispersion velocity. The former is typically larger for disks and dwarf irregulars and the latter is larger for dwarf ellipticals.

peting forces is estimated to be (E. Quataert, private communication)

$$\frac{F_{\text{rad}}}{F_{\text{ram}}} \sim \frac{\dot{M}_*}{\dot{M}} Z(1+z)^2, \quad (49)$$

where  $\dot{M}$  is the gas infall rate and  $\dot{M}_*$  is the star formation rate. This ratio is likely to obtain a maximum just below the shock-heating mass scale, preferably at  $z \sim 1-2$ , partly because this is where the suppression of flows and star formation by supernova feedback is expected to be minimal. This is also where  $M/L$  is observed to be at a minimum as a function of mass (§1, item k), and the star formation rate is at a maximum as a function of time (§1, item f).

Thus, the upper bound for UV-on-dust feedback coincides with the upper bound for dominant cold flows because they are both determined by the shock-heating scale. We note that this scale also practically coincides with the upper bound for supernova feedback, at least at low redshifts.

### 7.3. Photoionization feedback

The UV from the first stars and AGNs is believed to ionize most of the gas in the universe at  $z \sim 10$ , and provide an effective feedback mechanism in small halos (Loeb & Barkana 2001; Bullock et al. 2000; Somerville 2002; Benson et al. 2003). The gas that is uniformly heated to slightly above  $10^4 \text{ K}$  is prevented from falling into halos smaller than the Jeans mass of the ionized gas, corresponding to  $V_v \sim 30 \text{ km s}^{-1}$  (Thoul & Weinberg 1996; Quinn, Katz & Efstathiou 1996; Gnedin 2000). If the ionization persists for cosmological epochs, the hot gas gradually evaporates via steady thermal winds from halos smaller than a similar characteristic scale (Shaviv & Dekel 2003). While this feedback mechanism is likely to be relevant for explaining the faint-end of the luminosity function, (§9), it is unlikely to be important on larger scales closer to the shock-heating scale, where the virial velocity corresponds to  $T \sim 10^6 \text{ K}$ . In these halos the supernova feedback and the UV-on-dust feedback are expected to be the dominant feedback effects.

### 7.4. AGN feedback

The feedback processes addressed so far are effective in halos below the critical scale of  $\lesssim 10^{12} M_\odot$ . However, the upper limit to the stellar masses of galaxies, the indicated shut-down of star formation in big halos, the rising  $M/L$  in groups and clusters, and the absence of cooling flows in clusters, all require more energetic feedback sources that should be able to affect more massive halos.

The energy emitted from AGNs, as observed for example in their radio jets, is typically more than necessary for keeping a significant fraction of the halo gas hot. Given that the typical black hole mass is related to the dispersion velocity of the galaxy by  $M_{\text{BH}} \sim 10^7 M_\odot V_{100}^4$ , and assuming that a fraction  $\epsilon$  of the black hole mass has been radiated away during the black-hole growth, the ratio of total AGN energy to the gas binding energy is  $E_{\text{AGN}}/E_{\text{gas}} \sim 7 \times 10^3 \epsilon f_{b,0.05}^{-1} V_{100}^{-1}$ . If this ratio is a measure of the efficiency of the feedback process, it implies that the feedback efficiency is decreasing with halo mass. Nevertheless, for  $\epsilon > 10^{-3}$  there seems to be enough AGN energy for affecting most of the halo gas, even in cluster halos of  $V_{100} \sim 10$ .

The challenge is to figure out how the energy released on the "microscopic" black-hole scale is transferred into the

halo gas spread over a much larger volume. Preliminary attempts at investigating possible mechanisms, e.g. appealing to the formation of large bubbles and their buoyancy outward, are being made in the context of preventing cooling flows in clusters (Ruszkowski, Bruggen & Begelman 2004; Begelman 2004), as well as concerning galaxy formation (Scannapieco & Oh 2004). However, the detailed physics of AGN feedback is not yet fully understood. We are limited to crude estimates to be taken with a grain of salt, and should be guided by observational clues.

AGNs are observed to exist preferentially in halos above the critical mass of a few times  $10^{11} M_\odot$ , where the spheroids tend to be massive, the galaxies tend to be grouped, and the gas is expected to be shock heated. It is possible that this is associated with a minimum bound for the mass of halos or spheroids hosting black holes, reflecting a minimum for the mass of the black holes themselves (Koushiappas, Bullock & Dekel 2004). Alternatively, the black holes may exist also below the critical mass, but they somehow do not release significant energy as AGNs today. This may be due to starving the black holes by the feedback mechanisms working below the critical mass, such as supernova feedback or radiation-on-dust, allowing them to shine only when the halo becomes more massive than the critical mass.

No matter how the actual AGN feedback mechanism works, it is likely that the shock heating of the gas into a dilute medium makes it vulnerable to heating and/or pushing by the central energy source, thus providing the trigger for making the feedback effective.

In this case, the feedback efficiency can be expected to be less sensitive to the actual energy released by the AGN, given that it is always sufficient. Instead, the feedback efficiency is determined by the relative fractions of hot and cold gas in the halo. Appealing to cosmological simulations, we read from Fig. 3 that near the critical mass the hot fraction varies roughly in proportion to  $M^{1/2}$ . This can provide an estimate for the variation of mass-to-light ratio as a function of mass in halos just above the critical mass,  $M/L \propto M^{1/2}$ , in qualitative agreement with the observed trend (§1, item k).

### 7.5. Two-phase Medium

Given that the cooling function has a peak near  $\sim 10^4 \text{ K}$ , the gas that has been shock heated to near the virial temperature of  $\gtrsim 10^6 \text{ K}$  becomes thermally unstable; it is likely to develop a two-phase medium, with cold, dense clouds that are pressure confined within the hot, dilute medium (Field 1965; Fall & Rees 1985; Murray & Lin 1990). The distribution of cloud sizes, and the relevant time scales for their evolution and destruction, are affected by thermal conductivity as well as by dynamical processes (in the context of cluster cooling flows Voigt & Fabian 2004). Maller & Bullock (2004) have argued that under realistic conditions, this multi-phase phenomenon may have important effects in big galaxies. However, it has not yet been properly resolved in simulations on galactic scales, and it is not clear yet how this process is affected by the gravitational clumpiness of the dark-matter halo.

The multi-phase medium acts like a "feedback" process in the sense that it slows down the gas accretion rate into the inner disk, and can thus help explaining the bright-end truncation of the galaxy luminosity function and the other phenomena commonly addressed by other feedback processes. On one hand, a significant fraction of the gas may be locked

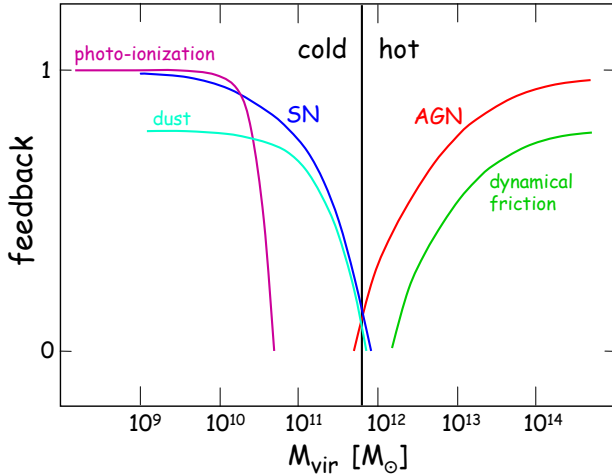


FIG. 8.— The “strength” of the various feedback processes at  $z = 0$ , e.g. referring to the fraction of the initial gas that has been heated or removed (schematic). Different feedback processes are effective below and above the critical shock-heating scale  $\lesssim 10^{12} M_{\odot}$ , and the feedback efficiency is at a minimum near this scale, giving rise to a minimum in  $M/L$  there. Recall that groups start appearing above  $10^{12} M_{\odot}$ .

for several dynamical times in the cold clouds that orbit the dark halo in low-eccentricity orbits. On the other hand, the density of the hot gas  $\rho_{\text{hot}}$  becomes lower, which makes its cooling time longer in proportion, thus slowing its quasi-static infall rate. Approximating eq. (17) with  $t_{\text{cool}}/t_{\text{comp}} \propto \rho^{-1} T_v^2$ , and recalling that  $T_v \propto M_v^{2/3}$ , we find that the longer cooling time makes the critical mass for further shock heating (where  $t_{\text{cool}}/t_{\text{comp}} \sim 1$ ) smaller by a similar factor,  $M_{\text{shock}} \propto \rho_{\text{hot}}^{3/4}$  (same as  $M_{\text{shock}} \propto f_b^{3/4}$  in eq. (34)). This means that for halos just above the original shock-heating mass, the development of a two-phase medium helps enhancing the shock stability. The hot gas may be kept hot over longer periods by repeating shocks due to continuous gas accretion into the halo. This may alleviate the need for other energetic feedback sources such as AGNs. However, much like the case of AGN feedback, a necessary condition for the two-phase medium to be effective in keeping the gas hot is the initial shock heating, i.e., being in a halo more massive than  $M_{\text{shock}}$ .

### 7.6. Dynamical-friction feedback

Yet another source for heating the gas in massive halos is the dynamical friction acting on the galaxies within a halo as they spiral into the halo center. The energy transferred to the gas by this process has been estimated to be comparable to that required for preventing cooling flows in cluster centers (El-Zant, Kim & Kamionkowski 2004). This energy source is valid once several massive galaxies move inside a common host halo, namely in groups and clusters of galaxies. The gas response to dynamical friction, unlike the DM response, has a sharp peak near a Mach number of unity (Ostriker 1999, Fig. 3), namely when the gas is heated to near the virial temperature in  $M > M_{\text{shock}}$  halos and not in smaller halos hosting much cooler gas. As groups occur above a critical halo mass that roughly coincides with the shock-heating scale at  $z \leq 1$  (§6), the dynamical-friction feedback appears almost simultaneously with the appearance of the hot medium, which then serves as the vulnerable victim of that feedback process. This is a common feature to all the feedback processes operating in massive halos.

### 7.7. Feedback summary

Figure 8 is a schematic illustration of the strength of each of the different feedback processes discussed here, crudely referring to the expected fraction of the initial gas that could have been heated or removed at  $z \sim 0$ . The curve for the supernova feedback is based on the energetics argument,  $M_s/M \propto V^2 \propto M^{2/3}$ . The strength of the AGN feedback is based on the rate of change from cold to hot infall in the simulations,  $M_{\text{cold}}/M \propto M^{-1/2}$ . The figure highlights the fact that different feedback processes dominate below and above the critical shock-heating scale of  $\lesssim 10^{12} M_{\odot}$ . As argued above, the transition from cold to hot infall has a crucial role in determining the different feedback efficiencies near the critical mass, though the scales associated with supernova feedback and with groups are also affected by independent sources (nuclear energy and dark-matter clustering respectively).

The point we emphasize here is that the feedback efficiency tends to have a minimum at a critical scale  $M_{\text{fdbk}} \sim M_{\text{shock}}$ . At higher redshifts this minimum becomes wider and therefore deeper, but it remains centered on a critical mass that is roughly the same at different redshifts. This gives rise to a minimum in  $M/L$  near this scale; in fact, the general shape of the schematic feedback diagram in Fig. 8 should resemble the general shape of the  $M/L$  function. In turn, it gives rise to a corresponding peak in the cosmological star formation rate at  $z \sim 1-2$  (see §8).

We conclude that at late epochs, the characteristic scales introduced by shock heating, by feedback, and by the clustering process, all roughly coincide, at  $\lesssim 10^{12} M_{\odot}$ . The implications must be far reaching, independent of whether this match of scales is causal or coincidental.

## 8. THE ORIGIN OF BI-MODALITY

We propose that the thermal processes described in §2-5, combined with the feedback and clustering processes discussed in §5-7, play a key role in producing the main observed features listed in §1. The different processes seem all to be associated (at moderate and low redshifts) with characteristic mass scales in the ball park of the observed critical scale. These are the shock-heating versus cold flow scale  $M_{\text{shock}}$  at  $z < 2$  (and  $M_{\text{stream}}$  at  $z > 2$ ), the clustering scale  $M_*$ , and the minimum-feedback scale  $M_{\text{fdbk}}$  (Figures 4, 7, and 8). We try to figure out how these processes join to produce the robust bi-modality features associated with this characteristic scale, involving quantities such as luminosity, color, star-formation rate and bulge-to-disk ratio as a function of halo mass and environment.

### 8.1. The fate of gas

Based on our qualitative understanding of the processes discussed above, we adopt the following sensible assumptions concerning the effects and fate of cold flows and hot gas in different halos:

(a) **A new mode of star formation.** The collisions of the (possibly clumpy) streams with the cold disk produce bursts of star formation, analogous to the bursts resulting from the collisions of two gaseous disks or cold gas clouds. Under the conditions which allow a cold flow, the collision is expected to produce an isothermal shock near the disk. The rapid cooling behind the shock generates a dense, cold slab in which the Jeans mass becomes small and stars can form efficiently.

While the detailed physics of star formation under these conditions is yet to be worked out, we dare to assume that the cold flows provide a new mode of star formation which may be responsible for much of the stars in the universe. It may behave like an enhanced quiescent mode in the disk leaving it intact without producing a big spheroid, or be more similar to the starbursts associated with mergers.

(b) **Hot forever.** Once halo gas in a massive halo is shock heated to near the virial temperature, it is no longer a source of cold gas supply for disk growth and star formation. This is because the hot medium is dilute, which, besides slowing down its cooling, makes it vulnerable to feedback effects from AGNs or comparable energy sources working in massive halos. The shock heating is assumed to *trigger* a shut-down of further disk growth and all modes of star formation in halos where cold streams do not prevail. Cold, dense clouds and streams could be better shielded against winds and ionizing radiation.

(c) **Cold streams in a hot medium.** As discussed in §5, the cold streams, which penetrate the hot medium in  $M_{\text{shock}} < M < M_{\text{stream}}$  halos, supply cold gas for further disk growth and (bursty) star formation. This occurs before the critical redshift when the clustering scale  $M_*$  becomes comparable to the shock heating scale, and preferentially in relatively isolated galaxies that are fed by unperturbed filaments. After this critical redshift, and especially in halos hosting groups and clusters, there is no gas supply by cold streams, and a complete shut-down of star formation can follow.

### 8.2. A scenario from the physical ingredients

The *bi-modality* in color (or stellar age, or SFR) and in bulge-to-disk ratio versus halo mass, and the correlation with the environment, all seem to emerge naturally when the above physical ingredients are put together. The gross features of the evolution along the blue sequence, the transition to the red sequence, and their extent at different redshifts, are illustrated schematically in Fig. 9. The scenario can be described as follows, focusing on the central role of cold flows versus hot media.

(a) **The blue sequence.** It is dominated by galaxies in halos below  $M_{\text{shock}}$ , which grow gravitationally by accretion and mergers, preferentially at high  $z$ , and are fed by cold flows. The continuous streaming of cold gas into the inner regions of such halos results in disk growth and efficient star formation. Clumpy streams produce sequences of collisions and starbursts, each of which might be indistinguishable from other gas-rich merger events.

Since these halos are also below the critical supernova (and radiative) feedback scale, the star formation is regulated by feedback and can be prolonged over cosmological times. Galaxies get very blue because of repeating episodes of starbursts, caused by the clumpy nature of the cold streams/mergers and the interplay between infall, starburst and outflow.

The mergers, occurring preferentially at high redshifts, and possibly other global disk instabilities, lead to the gradual growth of bulge components, while the continuing supply of external cold gas replenishes new disks around them; the typical configuration is therefore a spiral disk galaxy with a bulge component.

As the system grows, the older stars turn red, and the bulges grow, tilting the blue sequence toward somewhat redder colors

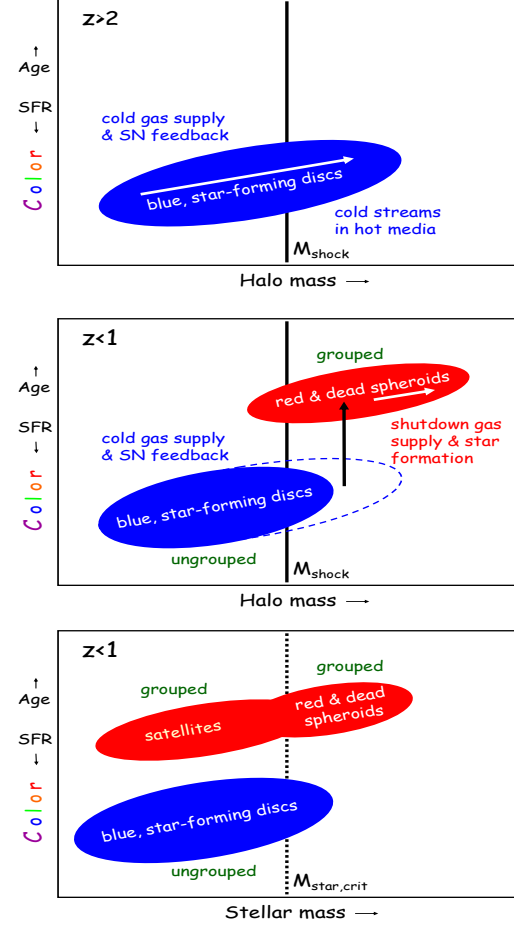


FIG. 9.— Schematic illustration of the origin of the bi-modality in color (or SFR or stellar age) as a function of halo mass. At  $z > 2$  (top), continuous gas supply, regulated by supernova feedback, makes the galaxies evolve along the blue sequence, which extends beyond the shock-heating mass due to cold streams in the hot media. At  $z < 1$  (middle), there are no cold streams above  $M_{\text{shock}}$ , the shock-heated gas is kept hot by AGN feedback, gas supply and star formation shut-down, and the stellar population passively turns red & dead. Gas-poor mergers stretch the red sequence toward larger masses. When the halo mass is replaced by stellar mass (bottom), the two ends of the red sequence are shifted down because  $M/M_*$  has a minimum near  $M_{\text{shock}}$ , and the red sequence is stretched toward small stellar masses due to the large population of satellite galaxies sharing a common halo. The color is correlated with the environment density via the halo mass, where the group mass is comparable to  $M_{\text{shock}}$ .

and larger bulges at higher masses.

At  $z < z_{\text{crit}}$ , the halos below  $M_{\text{shock}}$  are also below  $M_*$ , so the blue sequence is typically made of un-grouped halos hosting field galaxies in a low-density environment, which in turn does not perturb the cold-flow pattern and limits the major merger rate, thus allowing dominant disks.

(b) **Bright blue extension.** Some galaxies continue to be fed by cold streams even when they are more massive than  $M_{\text{shock}}$ , extending the blue sequence beyond  $M_*$ . This occurs especially at  $z > z_{\text{crit}}$ , when the streams are relatively narrow and dense, resulting in massive starbursts. This is valid when  $M_{\text{shock}}$  is sufficiently larger than  $M_*$ , namely earlier than  $z_{\text{crit}} \sim 1-2$ . At a given halo mass, this should occur preferably in relatively unclustered galaxies, where coherent streams can survive better and destructive major mergers are rare.

(c) **The red sequence.** Once a halo is more massive than  $M_{\text{shock}}$ , halo gas is shock heated; it becomes dilute and vulnerable to feedback effects. At  $z < z_{\text{crit}}$ , where cold streams

are suppressed, gas supply from the host halo shuts off, preventing any further growth of disks and the associated star formation.

These halos are also comparable to  $M_*$ , so they typically host groups, i.e. galaxies in high environment densities. Gaseous mergers were frequent during the assembly of such groups, while still on the blue sequence. They caused internal gas loss into starbursts and outflows, producing gas-poor spheroids, which are more stable against further star formation. These spheroids show up as big bulges preferentially at the red and massive end of the blue sequence. In parallel, the same mergers grew central black holes capable of providing feedback energy via AGN activity to couple effectively with the hot halo gas and keep it hot.

Thus, in the massive hot halos hosting groups at  $z < z_{\text{crit}}$ , *all* modes of star formation shut-down — the stellar population passively turns “red and dead” into the red sequence. The massive tip of the blue sequence at  $z > z_{\text{crit}}$  becomes the massive tip of the red sequence at  $z < z_{\text{crit}}$ . Subsequent growth along the red sequence is induced by mergers, which in such a halo tend to involve big, gas-poor spheroids and thus avoid contamination by new blue stars.

The bimodality induced by the shock heating in massive halos extends to smaller galaxies which are typically satellites of the central galaxies in common halos. In halos below  $M_{\text{shock}}$ , accretion onto satellite galaxies can keep them on the blue sequence for a while. In halos above  $M_{\text{shock}}$ , where gas supply stops and where the environment density is typically high, the satellites become red & dead.

### 8.3. Origin of each observed feature

Addressing the same scenario from the observational viewpoint, one can try to identify the physical processes responsible for each of the observed features listed in §1. Some of the discussion here is for the purpose of deepening our insight at the cost of being somewhat redundant to the previous subsection, while the rest of the discussion is addressing other observational features not addressed before. The main points are briefly summarized in Table 8.3.

The key to the whole *bi-modality* phenomenon is the early efficient star formation below the threshold halo mass followed by the abrupt shut-down in groups above this threshold.

The efficient star formation responsible for the *blue sequence*, below the critical halo mass and at all redshifts, is due to collisions of cold flows and disks or mergers of gas-rich disks. The *very blue* colors in certain small galaxies are due to the associated repeating episodes of starbursts. The appearance of *luminous starbursting* galaxies at  $z \geq 2$  (e.g. SCUBA sources) is due to cold streams which can penetrate hot halos above the shock-heating mass. [This would eliminate the need to appeal to hypothetical top-heavy IMF in star-bursts associated with high-redshift mergers (Baugh et al. 2004).]

The disappearance of these massive blue galaxies at  $z < 2$  and the appearance of luminous *extremely red* galaxies at  $z \leq 1$  is due to the abrupt shut-down of all modes of star formation, which eliminates any blue “froth” of young stars from contaminating the otherwise old and red population. This requires an efficient loss of gas from the galaxies themselves as well as a shut-down of the gas supply from the host halo, which could be achieved by mergers and by shock heating combined with AGN feedback respectively. This explains the *truncation* of the low-redshift (blue) galaxy luminosity func-

tion at the bright end beyond  $L_*$ . [This would eliminate the need for ad-hoc modifications in the modeling of the buildup of galaxies by merging satellites, involving a higher efficiency of tidal stripping and a reduced efficiency of dynamical friction (R. Somerville, private communication).]

The critical redshift at  $z_{\text{crit}} \sim 1-2$  is determined by the interplay between the gravitational clustering scale and the shock-heating scale.

The observed bi-modality in the *color-magnitude* diagram (§1, items a-d) emerges naturally from the color-mass bimodality predicted by the above scenario (Fig. 9). When the halo mass is replaced by stellar mass, the red sequence is shifted toward smaller masses relative to the blue sequence. The high-mass and low-mass ends move down because  $M/M_s$  has a minimum near the critical mass due to feedback effects (see below), and the sequence now extends toward small stellar masses, and develops a secondary bi-modality within it, due to the addition of red satellite galaxies sharing a halo with its other members. When the stellar mass is further replaced by luminosity or *magnitude*, given that  $M_s/L$  is higher for red galaxies, one expects a further broadening of the range over which the two sequences co-exist, highlighting the appearance of a gap between two peaks in the color distribution at a given magnitude. Note that the evolutionary tracks from the blue to the red sequence in the color-magnitude diagram are driven by passive aging into redder colors associated with luminosity fading toward fainter magnitudes.

A color *gap* is amplified by the fact that the galaxies “selected” for transition into the red sequence once the halo crosses the threshold mass tend to be those that populate the red, massive tip of the blue sequence, i.e. preferentially grouped merger remnants containing big gas-poor bulges as well as AGN feedback source. The color gap extends over a wide overlap region between the blue and red sequences when the halo mass is replaced by stellar luminosity.

The bi-modality in *bulge-to-disk ratio* is closely related. Some of the big spheroids in the red sequence should be the passively aged remnants of galaxies that have developed massive stellar components already in the blue sequence (rather than being the remnants of gas-poor mergers along the red sequence). The big spheroids make the transition because (a) they have consumed their gas in the same mergers that produced the spheroids, (b) these mergers tend to occur in big halos hosting groups, where shock heating stops the gas supply, and (c) these spheroids contain the massive black holes required for maintaining the halo gas hot. However, while the physics of shocks and the clustering process can both naturally give rise to the characteristic scale associated with the bi-modality, there is no obvious such scale emerging from the black-hole physics (except, perhaps, the possible starvation of AGNs by supernova feedback mentioned above).

The strong anti-correlation of *star-formation rate* (and blue color) with the number density of galaxies in the *environment* (§1, item h) is a natural outcome. The characteristic halo-mass predicted by gravity and by cooling processes for groups of galaxies is comparable to the shock-heating mass at  $z \leq 1$ . The predicted strong dependence of cold gas supply on host-halo mass can therefore be responsible for the distinction between the star formation rates in field and clustered galaxies. This distinction is predicted to be limited to late times. The galaxies dominating low-HOD halos below the critical shock mass today enjoy cold gas supply and are therefore dominated

TABLE 1  
THE ORIGINS OF SPECIFIC OBSERVATIONAL FEATURES

Observation	Origin
Blue sequence & fundamental line	Cold flows in $M < M_{\text{shock}}$ halos (+mergers); SFR regulated by (SN+radiative) feedback.
Big red & no big blue galaxies at $z \leq 1$	Shutdown SFR in $M > M_{\text{shock}}$ halos due to hot gas coupling with (AGN) feedback. Mergers in groups ( $> M_{\text{shock}}$ ) produce gas poor spheroids which helps the shut-down.
Big blue galaxies at $z \geq 2$	Cold streams in $M > M_{\text{shock}}$ ; critical $z$ defined by $M_{\text{shock}} \gtrsim M_*(z = z_{\text{crit}})$ .
Color bimodality gap	Abrupt shut-down of SFR; red sequence from reddish bright spheroids in the blue sequence. Wide overlap when luminosity replaces halo mass; satellites added to the red sequence
Environment dependence	Group halo mass $\sim M_* \sim M_{\text{shock}}$ ; SFR in $M < M_{\text{shock}}$ and shut-down in $M > M_{\text{shock}}$ .
Bulge/disk bimodality	Discs (& SFR) by cold flows in $M < M_{\text{shock}}$ halos, i.e. not groups. Discs become gas-poor bulges by mergers in groups, $M > M_{\text{shock}}$ , SFR off, turn red. Mergers in groups produce BH sources of AGN feedback, helps maintaining SFR shut-down.
$M/L$ minimum	Feedback minimum near $M_{\text{shock}}$ : $M_{\text{SN}} < M_{\text{shock}}$ while $M_{\text{AGN}} > M_{\text{shock}}$ .
SFR peaks at $z \sim 1$	Feedback minimum near $M_{\text{shock}}$ and $M_{\text{shock}} \sim M_*(z \sim 1)$ . Maximum cold flows in $M \sim M_{\text{shock}}$ at $z \geq 1.5$

by disks forming stars and a moderate rate of gas-rich mergers yielding a blue appearance. The galaxies populating groups of subhalos embedded in host halos are typically above the critical shock-heating mass at  $z \leq 1$  — they suffer starvation of external cold gas supply and lost their internal gas in mergers, thus stopped forming stars and passively evolved to the red sequence. The faint end of the red sequence, preferentially present in high environment densities, is due to the starvation of satellite galaxies in halos above  $M_{\text{shock}}$ , which are also typically of high HOD (along the lines of Berlind et al. 2004).

In fact, the classical *morphology-environment* relation, traditionally attributed to the correlation of merger rate with the environment, may also be partly viewed as a result of the cold-flow phenomenon. Instead of focusing on the destruction of disks and formation of spheroids, we note that big disks develop in big halos where cold streams prevail, i.e. only at  $z \geq 2$  and possibly in relatively isolated halos at later times. On the other hand disks cannot grow in big, group halos, where the cold streams are suppressed at late epochs. Then, the fact that major mergers are more frequent in forming groups helps building the big spheroids preferentially there. The morphology-environment correlation may be expected to be weaker than the color-environment correlation because the star-formation rate depends more directly on the environment via the halo mass, while the morphology arises from processes such as clumpy streams and mergers whose correlation with the environment is less direct.

The minimum in the mean halo *mass-to-light* ratio  $M/L$  near the critical mass  $\sim 10^{11-12} M_\odot$  (§1, item k) can be attributed to the minimum in gas supply near  $M_{\text{shock}}$  due to shock heating above this halo mass and the associated minimum in feedback effectiveness near this scale (Fig. 8). The

supernova and radiative feedback get stronger toward smaller halos, which explains the fundamental line defined by the structural properties of galaxies along the blue sequence (§1, item l). The AGN and dynamical-friction feedbacks, on the other hand, pump energy more effectively into the shock-heated medium that becomes more dominant toward more massive halos. The shut-down of gas supply by shock heating is responsible for the little growth of galaxy luminosities as a function of halo mass in groups and clusters (§1, item k). This minimum in gas supply near  $M_{\text{shock}}$  makes the halos near the critical scale the most efficient disk builders and star formers.

In fact, one can crudely predict the expected general shape of the  $M/L$  function about the minimum. Below the critical mass, the fundamental line due to supernova feedback corresponds to  $M/L \propto M^{-2/3}$  (Dekel & Woo 2003). As mentioned in §7 based on Fig. 3 due to the simulations of Keres et al. (2004), the transition from cold to hot infall as a function of mass indicates  $M/L \propto M^{1/2}$ . This is in the ballpark of the findings from 2dF (§1, item k), given the large uncertainties. The feedback effects can thus help resolving the discrepancy between the halo mass function and the galaxy luminosity function both at the bright end and below the bimodality/transition scale.

The fact that the color-magnitude bi-modality scale seems to be independent of redshift out to  $z \sim 1.5$  (§1 item d) is consistent with the model prediction (Fig. 7) that the critical halo mass is  $\sim 6 \times 10^{11} M_\odot$  roughly independent of redshift in this range. Further analyses of  $z \rightarrow 1.5$  surveys (such as the DEEP2/3 Madgwick et al. 2003; Coil et al. 2004) should reveal a similar behavior of  $M/L$  as a function of  $M$  as at  $z \sim 0$ .

Back to the issue of massive starbursts at high  $z$ . Besides the increased effect of cold flows in high-mass halos at  $z \geq 2$ , the

shock-heating halo mass itself may in fact be somewhat *larger* at high  $z$  due to a possible increase in the baryonic fraction  $f_b$  entering the cooling time. We assumed at  $z \sim 0$  a typical value of  $f_b \sim 0.05$ . However, as seen in Fig. 4 and summarized in §7.7, at high  $z$  the upper-limit mass for supernova feedback becomes smaller than the shock-heating mass, e.g., by a factor of  $\sim 4$  at  $z = 3$ . Therefore, in the mass range between the supernova mass and the shock mass, the cold gas supply is less interrupted by the two feedback processes, allowing a higher fraction of the gas to flow into the disk, perhaps as high as the universal value  $f_b \sim 0.13$ . Based on eq. (34), this corresponds to doubling the shock-heating halo mass. Another factor proportional to  $f_b$  may be introduced when translating to the corresponding stellar mass, yielding a total increase of  $\sim 5$  at high  $z$  in the critical stellar mass corresponding to shock heating. This is in addition to the increased efficiency of cold flows at high  $z$ , which drives the high star-formation rate there. One should therefore not be surprised by detections of strong star-formation activity at high  $z$  in halos exceeding  $\sim 10^{12} M_\odot$ , with virial velocities exceeding  $\sim 200 \text{ km s}^{-1}$  and with stellar masses exceeding  $\sim 10^{11} M_\odot$  (§1, item e).

The global *star formation history* could be derived from the predicted star formation efficiency as a function of mass and redshift, convolved with the time evolution of the halo mass function in the given cosmology. With the prediction that halos just below the shock-heating halo mass are the most efficient star formers, and with the Press-Schechter estimate that halos of such a mass typically form at  $z \sim 1$  (Fig. 4), the star formation density is predicted to peak near  $z \sim 1$ , with a relatively flat behavior toward higher redshifts and a sharp drop toward lower redshifts, as observed (§1, item f). In particular, the cumulative stellar density seems to stop growing quite abruptly at  $z \sim 1$  (Dickinson et al. 2003), when the typical forming halos become larger than the shock-heating scale and the cold flows are suppressed.

## 9. SHOCK HEATING IN SMALL HALOS

While we focused so far on the role of cold versus hot infall and feedback processes in producing the characteristic scale of big galaxies, we comment here on their role in giving rise to the two scales characterizing dwarf galaxies. One is the lower bound to observable dwarf galaxies at  $V_v \sim 10 \text{ km s}^{-1}$  (e.g., Dekel & Woo 2003, Fig. 3), and the other is the scale  $V_v \sim 30 \text{ km s}^{-1}$  below which most of the halos are likely to be “dark dark halos” (DDH) with no luminous trace.

The lower bound for dwarf galaxies at  $V_v \sim 10 - 15 \text{ km s}^{-1}$  is most likely related to the sharp drop in the atomic cooling rate just below  $\sim 10^4 \text{ K}$ , affecting the thermal history via shock heating in analogy to the phenomena responsible for the more massive shock-heating scale discussed above.

Figure 10 shows at the bottom panel the quantity relevant to shock stability, the rate ratio  $t_{\text{cool}}/t_{\text{comp}}$  given in eq. (17), versus its critical value at unity, as a function of halo mass, now stretching to low masses. The cooling rate is assumed here to be provided by atomic cooling alone, which drops sharply just below  $10^4 \text{ K}$ . The molecular-hydrogen cooling rate, which is needed for further cooling into star-formation temperatures, is neglected in this calculation, given that it is significantly weaker and may actually be eliminated altogether due to the efficient dissociation of the molecules in the presence of a UV background (Haiman et al. 1996). The stability is evaluated at  $z = 0$ , first in the disk vicinity,  $r = 0.1 R_v$ , assuming  $Z = 0.1$  and  $\tilde{u}_s = 0$ , and second near the virial radius, assuming  $Z = 0.03$

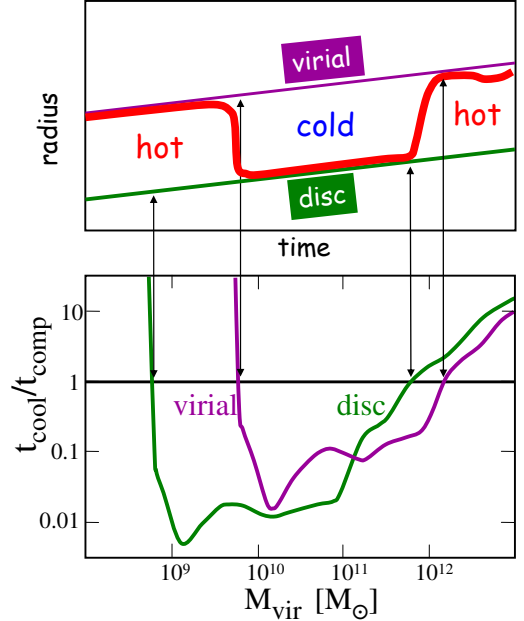


FIG. 10.— Shock stability as a function of mass at  $z = 0$ . Bottom: The ratio of rates,  $t_{\text{cool}}/t_{\text{comp}}$ , as a function of halo mass derived at the disk ( $Z = 0.1$ ,  $u_s = 0$ ) and at the virial radius ( $Z = 0.03$ ,  $u_s = 0.15$ ). The cooling rate is assumed to vanish for  $T < 10^4 \text{ K}$ . A stable shock is possible once  $t_{\text{cool}}/t_{\text{comp}} > 1$ . Top: A schematic illustration of the evolution of shock radius between the disk vicinity and the virial radius as the halo mass grows in time, based on the stability criterion shown in the bottom panel.

and  $\tilde{u}_s = 1/7$ . The range of stability at the low-mass end (where  $t_{\text{cool}}/t_{\text{comp}} \gg 1$ ), ending with the onset of instability at a few times  $10^9 M_\odot$ , is very relevant for the lower bound of dwarf galaxies.

The top panel of Fig. 10 illustrates the evolution of shock radius between the disk vicinity and the virial radius as the halo mass grows in time, based on the stability evaluated from the bottom panel. As long as the halo is below  $\sim 10^9 M_\odot$ , it has a stable shock near the virial radius. As the halo grows to  $\simeq 6 \times 10^8 M_\odot$ , the conditions near the disk become unfavorable for a stable shock, but the virial shock persists and the infalling gas is still heated to near the virial temperature. Only when the halo becomes  $\simeq 6 \times 10^9 M_\odot$  the virial shock disappears and shock heating stops completely. Then, in halos in the range  $6 \times 10^9 - 6 \times 10^{11} M_\odot$ , the gas flows cold into the halo center, leading to an efficient formation of a stellar disk. This is the halo mass range allowing disk formation today; it is quite narrow today and somewhat broader at high redshifts (Fig. 11). As discussed in §4.5, once the halo grows beyond the threshold mass, a stable shock propagates from the disk outward, reaching the virial radius at  $\sim 10^{12} M_\odot$  and remaining at the virial vicinity as the halo continues to grow.

The shock heating in halos smaller than a few times  $10^9 M_\odot$  prevents the formation of a stellar component even before the epoch of re-ionization by the first stars and AGNs. The inefficient cooling below  $10^4 \text{ K}$  allows the gas in such halos to maintain its virial temperature of  $\lesssim 10^4 \text{ K}$  for a long time. Once the first stars form in the dense centers of big clouds, their UV radiation reionizes the gas, dissociates molecules, and helps preventing cooling. This provides a natural explanation for the absence of observable galaxies below  $\sim 10^9 M_\odot$ , predicting a large population of mini halos which are completely dark.

Also in the dwarf range  $10 \leq V_v \leq 30 \text{ km s}^{-1}$ , most of the halos are likely to be DDHs with no luminous trace. This can be deduced from the discrepancy between the flat faint-end luminosity function of galaxies and the steep halo mass function predicted in  $\Lambda$ CDM, given the Tully-Fisher like velocity-luminosity relation of dwarf galaxies (e.g., Dekel & Woo 2003, Fig. 3). Independent evidence for DDHs comes from gravitational lensing (e.g. Dalal & Kochanek 2002).

While supernova feedback can be the primary process responsible for the fundamental line of dwarf galaxies between the two shock-heating scales, it is unlikely to be responsible for a complete removal of the gas from halos without leaving behind gaseous or stellar tracers. The complete evaporation of gas from halos of  $V_v < 30 \text{ km s}^{-1}$  can be explained by steady thermal winds (Shaviv & Dekel 2003) resulting from the cosmological photoionization starting at  $z \sim 10$ . The Jeans mass of the ionized IGM being of a comparable scale ensures that smaller halos do not accrete new gas as long as the IGM is highly ionized. This may explain the dominance of DDHs below  $\sim 30 \text{ km s}^{-1}$ , as well as the presence of gas-poor dwarf spheroidals whose old stars might have formed before the onset of reionization.

## 10. DISCUSSION: OTHER POSSIBLE IMPLICATIONS

We refer here to several possible implications of the cold-flow process described above, addressing open issues in galaxy formation, and proposing further study.

**X-rays.** The shock-heating scale may be directly detectable in soft X-rays, as the lower limit for galaxies and groups containing hot halo gas (§1, item j). In turn, the suppression of shock heating in halos below the threshold mass may help explaining the missing soft X-ray background problem (Pen 1999; Benson et al. 2000). The issue is that the observed flux (Cui et al. 1996), after subtracting the contribution of quasars, seems to be significantly lower than the flux predicted for halos in the standard  $\Lambda$ CDM cosmology under the assumption that *all* the halo gas is shock heated to the virial temperature. With no shock heating below the critical mass there should be a noticeable suppression of the predicted X-ray emission in the range  $5 \times 10^5$  to  $2 \times 10^6 \text{ K}$ , to be calculated in more detail elsewhere.

**Lyman-alpha emission.** The cold ( $\sim 10^4 \text{ K}$ ) gas streaming into the halos may instead be an efficient source of Ly- $\alpha$  radiation, possibly associated with observed Ly- $\alpha$  emitters at high redshift (Kurk et al. 2003, and references therein). It has been argued based on SPH simulations (Fardal et al. 2001; Furlanetto et al. 2003) that the flows radiate their infall energy mostly in Ly- $\alpha$  before they blend quite smoothly into the disks. Another possibility is that the supersonic streams do eventually shock at the inner halo near the disk, which does produce X rays there. However, given the high density at the disk vicinity, the generated X-ray radiation is likely to be confined to the inner halo; it is expected to ionize the gas inside a Strömgren sphere of a few kiloparsecs rather than escape from the halo. This energy will then be transformed into Ly- $\alpha$  radiation, which could propagate out of the halo via thermal broadening and systematic redshifts. A non-trivial study involving radiative transfer is required here.

**Damped Lyman-alpha systems.** Massive cold flows may be associated with the damped Lyman-alpha systems along the lines of sight to quasars (Prochaska et al. 2003, and references therein). It would be worthwhile to address the properties of

cold flows in cosmological simulations in this context.

**LIRGS.** Cold flows may also help explaining some of the massive starbursts associated with LIRGs at  $z \lesssim 1$  (Hammer et al. 2004). Given that about half the stars in today's disk galaxies were formed in these LIRGs, and that the majority of galaxies today are fragile disks, indicate that many of the LIRGs could not have been produced by violent major mergers. The cold streams may provide a less violent starburst mechanism that is not associated with the destruction of disks. Simulations that properly incorporate cold streams should be confronted with the data.

**Angular momentum.** The proposed scenario may set the stage for solving one of the main puzzles in galaxy-formation theory – the angular-momentum problem, characterized by the failure of current cosmological simulations to reproduce the observed population of disk galaxies. Instead, the simulations show significant angular-momentum transfer from the gas to the dark matter associated with an over-production of low-angular-momentum spheroids (Navarro & Steinmetz 2000). The solution should involve the removal of baryons with low specific angular momentum. In galaxies smaller than the critical mass, the supernova and radiative feedback can balance the gas cooling and blow the gas away from the small building blocks, which are otherwise the main source of low angular momentum via minor mergers coming from a mixture of orbits (Maller, Dekel & Somerville 2002; Maller & Dekel 2002). In galaxies on the order of the shock-heating mass, the low angular momentum gas is typically associated with the shock-heated medium inside the virial sphere, which can be prevented from cooling by AGN feedback. The cold streams, which are coherent and come from larger distances, are likely to carry high angular momentum, and they are capable of producing extended, bulge-free disks. We see such a behavior in cosmological hydro simulations (Zinger et al. 2005). We note in passing that according to this scenario, the spheroid formation is not simultaneous with the disk formation but is rather a result of disk mergers or a central bar losing its angular momentum, both predicting a correlation between the bulge-to-disk ratio and the galaxy mass, as observed (§1, item g). The key for solving the angular-momentum problem is thus efficient feedback mechanisms, both below the critical scale and slightly above it. These have not been properly simulated yet, partly because of an incomplete treatment of the micro-physics in most current simulations.

**Cold clouds.** The formation of the disk by a clumpy cold gas phase may have several interesting implications. (a) As mentioned above, it may help explaining the bursty nature of star formation responsible for the small very-blue galaxies observed at the tail of the blue sequence (§1, item b). (b) As discussed in §7.5, it may also help explaining the bright-end luminosity function discrepancy (§1, item k), by keeping some of the gas for longer periods both in a hot, dilute phase of long cooling times and in orbiting clouds (Maller & Bullock 2004). (c) The dynamical friction bringing the orbiting clouds into the disk is a mechanism for transferring energy from the disk into the inner halo, which may help explaining yet another major problem facing galaxy formation theory – the halo core problem. This is the apparent discrepancy between the steep inner cusps predicted by N-body simulations of CDM halos growing by gravity alone and the flat inner cores indicated by rotation curves in low-surface-brightness galaxies (Dekel, Devor & Hetzroni 2003; Dekel, Arad, Devor & Birnboim 2003;

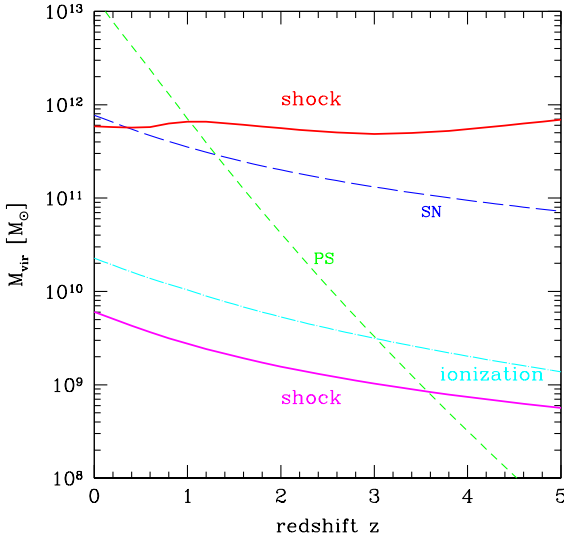


FIG. 11.— Summary of characteristic scales relevant to galaxy formation. Shock heating is expected above the upper curve where a stable shock grows from the inner halo to the virial radius, and below the lower curve where there is a stable shock at the virial radius. Cold flows are expected between these curves, giving rise to disk growth and star formation. Also marked are the upper limits for supernova feedback and evaporation by photoionization. The Press-Schechter curve marks the typical halo forming at the given redshift – a wide range of masses about this curve could form at different environments.

El-Zant, Hoffman, Primack, Combes & Shlosman 2004; Ma & Boylan-Kolchin 2004). (d) The same process may lower the predicted maximum rotation velocity in disk galaxies at a given luminosity, balancing the adiabatic contraction of the dark halo, and thus repair the zero-point offset in current models of the Tully-Fisher relation (e.g. Klypin et al. 2002; Abadi et al. 2003; Dutton et al. 2004). (e) It may also help explaining the measured lack of anti-correlation between the residuals in velocity and radius at a given luminosity (Courteau & Rix 1999), indicating that the disks are not self-gravitating, with a comparable contribution of the dark halo to the gravitational potential at the effective disk radius (Dutton et al. 2004).

**Dust lane.** It has been noticed from a survey of edge-on disks that there is a sharp transition in the structure of their dusty interstellar medium at a characteristic scale of  $V_v \simeq 120 \text{ km s}^{-1}$  (Dalcanton, Yoachim & Bernstein 2004), comparable to the critical scale discussed in this paper. While more massive disks show a well-defined dust lane, in less massive galaxies the dust is distributed diffusely above and below the disk, possibly supported by turbulence. A turbulent dusty gas phase of a large scale height is indeed expected when supernova feedback is effective, and when cold streams shock near the disk and produce stars, namely below a threshold which coincides with the observed scale. This deserves a detailed theoretical study.

## 11. CONCLUSION

### 11.1. Summary of results

The classic argument of cooling on a dynamical time scale (Rees & Ostriker 1977; White & Rees 1978), with order-of-magnitude estimates of the time scales involved, provided an inspiring qualitative upper bound for luminous galaxies, at a halo mass of  $M \sim 10^{12-13} M_\odot$ . An analytic study of the actual shock-heating process (Birnboim & Dekel 2003, and this paper) now yields a more concrete halo critical scale at

$M \simeq 6 \times 10^{11} M_\odot$ , somewhat smaller than the original estimate. The criterion for critical shock stability,

$$t_{\text{cool}}^{-1} = t_{\text{comp}}^{-1}, \quad (50)$$

is a balance between the cooling rate and the post-shock compression rate, which restores the pressure supporting the shock against gravitational collapse. The compression time is somewhat larger than the crossing time at the shock position. The absolute magnitudes of these time scales are irrelevant – they could in principle both be longer than the Hubble time, because what matters for shock heating versus cold flows is only the relative rates of the competing processes. The most relevant critical scale is obtained in the inner halo, because as the halo grows, the shock first becomes stable in the inner halo, and it then propagates outward to the virial radius. Halos of mass below the threshold mass build disks in their centers by cold flows, while in halos above the threshold much of the gas is shock-heated. These results are confirmed by spherical hydrodynamical simulations. The same phenomenon is seen at a comparable scale in general cosmological hydrodynamical simulations. They reveal that in halos near the critical scale, and even in larger halos preferentially at  $z \geq 2$  and especially in field galaxies, cold streams along the filaments feeding the galaxy penetrate through the hot medium, and allow further disk growth and star formation.

The interplay between these cold flows and shock-heating, the gravitational clustering scale, and the different feedback processes acting below and above a similar mass scale, is proposed to be responsible for the robust bi-modality imprinted on the observed galaxy properties. Cold flows in halos much bigger than the clustering scale allow massive starbursts at  $z \geq 2$ , while shock heating in comparable halos at later times shuts off star formation and leads to big red galaxies. While supernova and radiative feedbacks regulate star formation below the critical scale, the presence of dilute, shock-heated gas in more massive halos allows the AGN feedback (or another energetic source capable of affecting big galaxies) to keep the shock-heated gas hot and prevent further disk growth and star formation. The observed bi-modality and many of the related phenomena are argued to arise naturally from such a scenario (§8).

The shock-heating process also plays a role in introducing a lower bound to halos hosting galaxies, at  $\sim 10^9 M_\odot$ . The main characteristic scales in galaxy formation are summarized in Fig. 11 as a function of redshift. The mass range where disk galaxies form turns out to be quite narrow, between a few times  $10^9 M_\odot$  to slightly below  $10^{12} M_\odot$ .

### 11.2. Re-engineering of SAMs

Once the new physical processes discussed above are properly incorporated in the detailed models of galaxy formation, the hope is that they will solve many of the apparent conflicts between theory and observation. At a crude level, one might have naively thought that since the cooling time is anyway assumed to be short in small halos and long in big halos, the details of the cold-flow and shock-heating phenomena described above would not matter much to the final result. However, a closer inspection reveals that there are several key features which should make a qualitative difference in the SAMs:

(a) **Star formation.** The near-supersonic cold streams provide a new efficient mechanism for early star formation. This is in contrast to the gradual infall of cooling shock-heated gas

assumed in most SAMs, which starts from near rest, accretes smoothly into the disk, and joins the quiescent mode of star formation there. We find that the expected cold-gas supply is significantly more efficient than assumed in most current models even in small halos (Cattaneo, Neistein, Birnboim & Dekel, in preparation).

(b) **Heating inside out.** The concept of an expanding “cooling radius” used in current SAMs is limited to massive halos where a virial shock exists. Otherwise, it is the shock causing the heating which is propagating from the inside out.

(c) **Shutdown of star formation.** The combination of shock heating and AGN feedback provides a mechanism for shutting off disk growth and star formation above a threshold halo mass.

(d) **Cold streams.** Cold streams that penetrate through the hot media continue to make disks and produce stars in halos above the shock-heating mass. This happens mostly at  $z \geq 2$ , and preferentially in less grouped galaxies, allowing big blue galaxies mostly at high  $z$  and some at low-density environments, and enforcing a sharp shut-down of star formation at late times and especially in clustered galaxies.

A practical schematic recipe for the critical halo mass below which cold streams prevail and above which one may assume a shut-down of gas supply and star formation is:

$$M_{\text{crit}} = \begin{cases} M_{\text{shock}}, & z < z_{\text{crit}} \\ M_{\text{shock}} \left( \frac{M_{\text{shock}}}{f M_{*}(z)} \right), & z > z_{\text{crit}} \end{cases} \quad (51)$$

where the critical redshift  $z_{\text{crit}}$  is defined by  $f M_{*}(z_{\text{crit}}) = M_{\text{shock}}$ , the clustering scale  $M_{*}(z)$  is given by eq. (A18), and  $f$  is a numerical factor of order a few. Our best estimates for the parameters are  $\log M_{*} \simeq 11.8$  (but possibly another value in the range 11.3-12.3) and  $f \simeq 3$  (possible range: 1-10). Using the approximation  $\log M_{*} \simeq 13.1 - 1.3z$  ( $z \leq 2$ ), we obtain  $z_{\text{crit}} \simeq 1.4$  for  $f = 3$ . This recipe should allow big blue systems at  $z \geq 2$ , eliminate big blue systems and make big red galaxies at  $z \leq 1$ , and generate a bi-modality near  $M_{\text{shock}}$ . This scheme can be refined to allow for a smooth transition above the critical scale by applying the shut-down to a varying fraction of the gas and by breaking the streams into clumps which will generate high peaks of starbursts.

In addition, one may wish to have an effective minimum requirement for the central black-hole mass in order to ensure enough feedback energy for maintaining the gas hot. This may emphasize the bi-modality gap in color and bulge-to-disk ratio. However, the proposed shut-down by halo mass may be enough for ensuring sufficient bulge mass and black-hole mass.

The SAMs should be re-engineered to incorporate these processes and thus help working out the detailed implications of the proposed scenario. Preliminary attempts to do that, using two different SAMs, indicate that the incorporation of the new proposed processes outlined above indeed leads to significantly better fits with the observed bi-modality features along the lines proposed in §8. In particular, the introduction of a redshift-dependent halo-mass threshold has a robust effect on the color-magnitude diagram at different redshifts, as expected (Cattaneo et al. 2005).

### 11.3. Two Open issues

In parallel, the physics of the involved ingredients should be properly worked out in more detail, starting with the following two hypotheses that were laid out in §8.1.

(a) **Fate of cold streams.** A detailed investigation is required of the way by which the cold streams evolve and eventually merge with the central disk, the associated star formation, and the resulting feedback process. While progress can be made using toy models and simplified simulations, a proper analysis will require simulations of higher resolution than are currently available. In particular, whether or not the predicted star bursts could be associated with the big dusty sources indicating massive star formation at high redshifts, such as the SCUBA sources (Chapman et al. 2003), remains to be determined once the theory is worked out and the observed characteristics of these sources are clarified.

(b) **AGN feedback.** The physics of AGN feedback is another unknown. One wishes to understand how the available energy originating near the central black hole is transferred to the hot gas spread over the halo. The physics of how thermal conductivity may heat the gas is also to be investigated. The increased efficiency of these feedback mechanisms in the presence of a hot medium as opposed to their effect on cold flows and clumps are to be quantified.

Parallel attempts to work out the details of the physical input and to incorporate it in more quantitative models of galaxy formation should lead to progress in our understanding of the galaxy bi-modality and the associated features.

We thank A. Kravtsov and R. Dave, N. Katz, D. Keres & D. Weinberg for sharing with us the results of their cosmological hydrodynamical simulations. We acknowledge stimulating discussions with J. Binney, A. Cattaneo, S.M. Faber, D. Lin, G. Kauffmann, G. Mamon, E. Neistein, J.P. Ostriker, J.R. Primack, R. Somerville & D. Weinberg. This research has been supported by ISF 213/02 and NASA ATP NAG5-8218. AD acknowledges support from a Miller Visiting Professorship at UC Berkeley, a Visiting Professorship at UC Santa Cruz, and a Blaise Pascal International Chair by Ecole Normale Supérieure at the Institut d’Astrophysique, Paris.

APPENDIX  
USEFUL RELATIONS

We summarize here the cosmological relations used in the analysis of §4. This is rather basic material, based for example on Lahav, Rees, Lilje & Primack (1991); Carroll, Press & Turner (1992) and Mo & White (2002). By specifying it here in a concise and convenient form, we hope to allow the reader to reproduce our results and use them in future analyses. Additional relations associated with the spherical top-hat collapse model are brought in the appendix of BD03.

*Cosmology*

The basic parameters characterizing a flat cosmological model in the matter era are the current values of the mean mass density parameter  $\Omega_m$  and the Hubble constant  $H_0$ . At the time associated with expansion factor  $a = 1/(1+z)$ , the vacuum-energy density parameter is  $\Omega_\Lambda(a) = 1 - \Omega_m(a)$  and

$$\Omega_m(a) = \frac{\Omega_m a^{-3}}{\Omega_\Lambda + \Omega_m a^{-3}}. \quad (\text{A1})$$

The Hubble constant is

$$H(a) = H_0 (\Omega_\Lambda + \Omega_m a^{-3})^{1/2}, \quad (\text{A2})$$

and the age of the universe is

$$t_{\text{univ}}(a) = \frac{2}{3} H(a)^{-1} \frac{\sinh^{-1}(|1 - \Omega_m(a)|/\Omega_m(a))^{1/2}}{(|1 - \Omega_m(a)|)^{1/2}}. \quad (\text{A3})$$

The mean mass density is

$$\rho_u \simeq 1.88 \times 10^{-29} \Omega h^2 a^{-3} \simeq 2.76 \times 10^{-30} \Omega_{m0.3} h_{0.7}^2 a^{-3}, \quad (\text{A4})$$

where  $\Omega_{m0.3} \equiv \Omega_m/0.3$ ,  $h \equiv H_0/100 \text{ km s}^{-1} \text{ Mpc}^{-1}$ , and  $h_{0.7} \equiv h/0.7$ .

*Virial relations*

The virial relations between halo mass, velocity and radius,

$$V_v^2 = \frac{GM_v}{R_v}, \quad \frac{M_v}{\frac{4\pi}{3} R_v^3} = \Delta \rho_u \quad (\text{A5})$$

become

$$M_{11} \simeq 6.06 V_{100}^3 A^{3/2} \simeq 342 R_{Mpc}^3 A^{-3}, \quad (\text{A6})$$

where  $M_{11} \equiv M_v/10^{11} M_\odot$ ,  $V_{100} \equiv V_v/100 \text{ km s}^{-1}$ ,  $R_{Mpc} \equiv R_v/1 \text{ Mpc}$ , and

$$A \equiv (\Delta_{200} \Omega_{m0.3} h_{0.7}^2)^{-1/3} a. \quad (\text{A7})$$

An approximation for  $\Delta(a)$  in a flat universe (Bryan & Norman 1998) is:

$$\Delta(a) \simeq (18\pi^2 - 82\Omega_\Lambda(a) - 39\Omega_\Lambda(a)^2)/\Omega_m(a). \quad (\text{A8})$$

The virial temperature can be defined by

$$\frac{kT_v}{m} = \frac{1}{2} V_v^2. \quad (\text{A9})$$

For an isotropic, isothermal sphere, this equals  $\sigma^2$ , where  $\sigma$  is the one-dimensional velocity dispersion and the internal energy per unit mass is  $e = (3/2)\sigma^2$ . Thus

$$V_{100}^2 \simeq 2.79 T_6 \quad M_{11} \simeq 28.2 T_6^{3/2} A^{3/2}, \quad (\text{A10})$$

where  $T_6 \equiv T_v/10^6 \text{ K}$ .

*Press Schechter*

Linear fluctuation growth is given by (Lahav et al. 1991; Carroll et al. 1992; Mo & White 2002)

$$D(a) = \frac{g(a)}{g(1)} a, \quad (\text{A11})$$

where

$$\begin{aligned} g(a) \simeq & \frac{5}{2} \Omega_m(a) \\ & \times \left[ \Omega_m(a)^{4/7} - \Omega_\Lambda(a) + \frac{(1 + \Omega_m(a)/2)}{(1 + \Omega_\Lambda(a)/70)} \right]^{-1}. \end{aligned} \quad (\text{A12})$$

The CDM power spectrum is approximated by (Bardeen et al. 1986):

$$P(k) \propto k T^2(k), \quad (\text{A13})$$

with

$$T(k) = \frac{\ln(1+2.34q)}{2.34q} \times [1+3.89q+(16.1q)^2+(5.46q)^3+(6.71q)^4]^{-1/4}, \quad (\text{A14})$$

where

$$q = k/(\Omega_m h^2 Mpc^{-1}). \quad (\text{A15})$$

It is normalized by  $\sigma_8$  at  $R = 8 h^{-1} \text{Mpc}$ , where

$$\sigma^2(R) = \frac{1}{2\pi} \int_0^\infty dk k^2 P(k) \tilde{W}^2(kR), \quad (\text{A16})$$

and with the Fourier transform of the top-hat window function

$$\tilde{W}(x) = 3(\sin x - x \cos x)/x^3. \quad (\text{A17})$$

In the Press Schechter (PS) approximation, the characteristic halo mass  $M_*(a)$  is defined as the mass of the  $1-\sigma$  fluctuation,

$$1 = \nu(M, a) = \frac{\delta_c}{D(a) \sigma(M)}, \quad \delta_c \simeq 1.69, \quad (\text{A18})$$

where  $M$  and the comoving radius  $R$  are related via the universal density today:  $M = \frac{4\pi}{3} \bar{\rho}_0 R^3$ . The mass of  $2-\sigma$  fluctuations is obtained by setting  $\nu(M, a) = 2$ , etc. Based on the improved formalism of Sheth & Tormen (2002), the fraction of total mass in halos of masses exceeding  $M$  is

$$F(> M, a) \simeq 0.4 \left( 1 + \frac{0.4}{\nu^{0.4}} \right) \operatorname{erfc} \left( \frac{0.85 \nu}{\sqrt{2}} \right). \quad (\text{A19})$$

This fraction for  $1-\sigma$ ,  $2-\sigma$ , and  $3-\sigma$  fluctuations is 22%, 4.7%, and 0.54% respectively.

Figure 4 shows the PS mass  $M_*$  as a function of redshift. For the standard  $\Lambda$ CDM with  $\sigma_8 = 0.9$  its value at  $z = 0$  is  $M_{*0} = 1.36 \times 10^{13} M_\odot$ . One can see that an excellent practical fit in the range  $0 \leq z \leq 2$  is provided by a power law in this semi-log plot:  $\log M_* \approx 13.134 - 1.3z$ . At larger redshifts this gradually becomes an underestimate. Trying to provide crude power-law approximations, we find that  $M_* \propto a^{4.2} \propto t^{3.5}$  are crude approximations in the range  $0 \leq z \leq 1$ , and that  $M_* \propto a^5 \propto t^4$  are good to within a factor of 2 in the range  $0 \leq z \leq 2$ . These power laws become overestimates at higher redshifts.

## REFERENCES

Abadi M. G., Navarro J. F., Steinmetz M., Eke V. R., 2003, ApJ, 591, 499  
 Abazajian K., Zheng Z., Zehavi I., Weinberg D. H., Frieman J. A., Berlind A. A., Blanton M. R., et al., 2004, astro-ph/0408003  
 Baldry I. K., Glazebrook K., Brinkmann J., Ivezić Ž., Lupton R. H., Nichol R. C., Szalay A. S., 2004, ApJ, 600, 681  
 Balogh M., Eke V., Miller C., Lewis I., Bower R., Couch W., Nichol R., et al., 2004, MNRAS, 348, 1355  
 Bardeen J. M., Bond J. R., Kaiser N., Szalay A. S., 1986, ApJ, 304, 15  
 Baugh C. M., Lacey C. G., Frenk C. S., Granato G. L., Silva L., Bressan A., Benson A. J., S. C., 2004, astro-ph/0406069  
 Begelman M. C., 2004, in Coevolution of Black Holes and Galaxies AGN Feedback Mechanisms, pp 375–+  
 Bell E. F., Baugh C. M., Cole S., Frenk C. S., Lacey C. G., 2003, MNRAS, 343, 343  
 Bell E. F., McIntosh D. H., Katz N., Weinberg M. D., 2003a, ApJ, 585, L117  
 Bell E. F., McIntosh D. H., Katz N., Weinberg M. D., 2003b, ApJS, 149, 289  
 Bell E. F., Wolf C., Meisenheimer K., Rix H., Borch A., Dye S., Kleinheinrich M., et al., 2004, ApJ, 608, 752  
 Benson A. J., Bower R. G., Frenk C. S., Lacey C. G., Baugh C. M., Cole S., 2003, ApJ, 599, 38  
 Benson A. J., Bower R. G., Frenk C. S., White S. D. M., 2000, MNRAS, 314, 557  
 Benson A. J., Frenk C. S., Baugh C. M., Cole S., Lacey C. G., 2003, MNRAS, 343, 679  
 Berlind A. A., Blanton M. R., Hogg D. W., Weinberg D. H., Davé R., Eisenstein D. J., Katz N., 2004, astro-ph/0406633  
 Binney J., 1977, ApJ, 215, 483  
 Binney J., 2004, MNRAS, 347, 1093  
 Binney J., Tremaine S., 1987, Galactic dynamics. Princeton, NJ, Princeton University Press, 1987, 747 p.  
 Birnboim Y., Dekel A., 2003, MNRAS, 345, 349  
 Blanton M. R., Eisenstein D., Hogg D. W., Schlegel D. J., Brinkmann J., 2003, astro-ph/0310453  
 Blanton M. R., Eisenstein D., Hogg D. W., Zehavi I., 2004, astro-ph/0411037  
 Blumenthal G. R., Faber S. M., Primack J. R., Rees M. J., 1984, Nature, 311, 517  
 Bullock J. S., Kolatt T. S., Sigad Y., Somerville R. S., Kravtsov A. V., Klypin A. A., Primack J. R., Dekel A., 2001, MNRAS, 321, 559  
 Bullock J. S., Kravtsov A. V., Weinberg D. H., 2000, ApJ, 539, 517  
 Carroll S. M., Press W. H., Turner E. L., 1992, ARA&A, 30, 499  
 Cattaneo A., Neistein A., Dekel A., 2005, in preparation  
 Chapman S. C., Blain A. W., Ivison R. J., Smail I. R., 2003, Nature, 422, 695  
 Chapman S. C., Smail I., Blain A. W., Ivison R. J., 2004, ApJ, 614, 671  
 Ciotti L., Pellegrini S., Renzini A., D’Ercole A., 1991, ApJ, 376, 380  
 Coil A. L., Davis M., Madgwick D. S., Newman J. A., Conselice C. J., Cooper M., Ellis R., et al., 2004, ApJ, 609, 525  
 Courteau S., MacArthur L. A., Dekel A., van den Bosch F., McIntosh D. H., Dale D., 2004, astro-ph/0310440  
 Courteau S., Rix H., 1999, ApJ, 513, 561  
 Cui W., Sanders W. T., McCammon D., Snowden S. L., Womble D. S., 1996, ApJ, 468, 117  
 Dalal N., Kochanek C. S., 2002, ApJ, 572, 25  
 Dalcanton J. J., Yoachim P., Bernstein R. A., 2004, ApJ, 608, 189  
 De Lucia G., Kauffmann G., White S. D. M., 2004, MNRAS, 349, 1101  
 Dekel A., 1981, A&A, 101, 79  
 Dekel A., Arad I., Devor J., Birnboim Y., 2003, ApJ, 588, 680  
 Dekel A., Devor J., Hetzroni G., 2003, MNRAS, 341, 326  
 Dekel A., Silk J., 1986, ApJ, 303, 39  
 Dekel A., Woo J., 2003, MNRAS, 344, 1131  
 Dickinson M., Papovich C., Ferguson H. C., Budavári T., 2003, ApJ, 587, 25  
 Ding J., Charlton J. C., Bond N. A., Zonak S. G., Churchill C. W., 2003, ApJ, 587, 551

Dressler A., 1980, *ApJ*, 236, 351

Dutton A., van den Bosch F. C., Courteau S., Dekel A., 2004, astro-ph/0501256

El-Zant A. A., Hoffman Y., Primack J., Combes F., Shlosman I., 2004, *ApJ*, 607, L75

El-Zant A. A., Kim W., Kamionkowski M., 2004, astro-ph/0403696

Fall S. M., Efstathiou G., 1980, *MNRAS*, 193, 189

Fall S. M., Rees M. J., 1985, *ApJ*, 298, 18

Fardal M. A., Katz N., Gardner J. P., Hernquist L., Weinberg D. H., Davé R., 2001, *ApJ*, 562, 605

Ferguson H. C., Babul A., 1998, *MNRAS*, 296, 585

Field G. B., 1965, *ApJ*, 142, 531

Fioc M., Rocca-Volmerange B., 1999, *A&A*, 344, 393

Furlanetto S. R., Schaye J., Springel V., Hernquist L., 2003, *ApJ*, 599, L1

Gao L., White S. D. M., Jenkins A., Stoehr F., Springel V., 2004, *MNRAS*, pp 484—

Giavalisco M., Dickinson M., Ferguson H. C., Ravindranath S., Kretchmer C., Moustakas L. A., Madau P., et al., 2004, *ApJ*, 600, L103

Gnedin N. Y., 2000, *ApJ*, 542, 535

Haiman Z., Rees M. J., Loeb A., 1996, *ApJ*, 467, 522

Hammer F., Flores H., Elbaz D., Zheng X. Z., Liang Y. C., Cesarsky C., 2004, astro-ph/0410518

Hartwick F. D. A., 2004, *ApJ*, 603, 108

Heavens A., Panter B., Jimenez R., Dunlop J., 2004, *Nature*, 428, 625

Helsdon S. F., Ponman T. J., 2003, *MNRAS*, 340, 485

Hickson P., Kindl E., Huchra J. P., 1988, *ApJ*, 331, 64

Hogg D. W., Blanton M. R., Eisenstein D. J., Gunn J. E., Schlegel D. J., Zehavi I., Bahcall N. A., et al., 2003, *ApJ*, 585, L5

Kannappan S. J., 2004, *ApJ*, 611, L89

Kauffmann G., Heckman T. M., Tremonti C., Brinchmann J., Charlot S., White S. D. M., Ridgway S. E., et al., 2003, *MNRAS*, 346, 1055

Kauffmann G., Heckman T. M., White S. D. M., Charlot S., Tremonti C., Peng E. W., Seibert M., et al., 2003, *MNRAS*, 341, 54

Kauffmann G., White S. D. M., Heckman T. M., Menard B., Brinchmann J., Charlot S., Tremonti C., Brinkmann J., 2004, astro-ph/0402030

Keres D., Katz N., Weinberg D. H., Dave R., 2004, astro-ph/0407095

Klypin A., Zhao H., Somerville R. S., 2002, *ApJ*, 573, 597

Koushiappas S. M., Bullock J. S., Dekel A., 2004, astro-ph/0311487

Kravtsov A. V., 2003, *ApJ*, 590, L1

Kravtsov A. V., Berlin A. A., Wechsler R. H., Klypin A. A., Gottloeber S., Allgood B., Primack J. R., 2004, astro-ph/0308519

Kravtsov A. V., Gnedin O. Y., 2004, astro-ph/0305199

Kurk J., Röttgering H., Pentericci L., Miley G., Overzier R., 2003, *New Astronomy Review*, 47, 339

Lahav O., Rees M. J., Lilje P. B., Primack J. R., 1991, *MNRAS*, 251, 128

Lin Y., Mohr J. J., 2004, astro-ph/0408557

Loeb A., Barkana R., 2001, *ARA&A*, 39, 19

Ma C., Boylan-Kolchin M., 2004, astro-ph/0403102

Madau P., Ferguson H. C., Dickinson M. E., Giavalisco M., Steidel C. C., Fruchter A., 1996, *MNRAS*, 283, 1388

Madgwick D. S., Coil A. L., Conselice C. J., Cooper M. C., Davis M., Ellis R. S., Faber S. M., et al., 2003, *ApJ*, 599, 997

Madgwick D. S., Somerville R., Lahav O., Ellis R., 2003, *MNRAS*, 343, 871

Maller A. H., Bullock J. S., 2004, astro-ph/0406632

Maller A. H., Dekel A., 2002, *MNRAS*, 335, 487

Maller A. H., Dekel A., Somerville R., 2002, *MNRAS*, 329, 423

Marinoni C., Hudson M. J., 2002, *ApJ*, 569, 101

Mathews W. G., Brightenti F., 2003, *ARA&A*, 41, 191

Mo H. J., Mao S., White S. D. M., 1998, *MNRAS*, 295, 319

Mo H. J., White S. D. M., 2002, *MNRAS*, 336, 112

Moustakas L. A., Casertano S., Conselice C. J., Dickinson M. E., Eisenhardt P., Ferguson H. C., Giavalisco M., et al., 2004, *ApJ*, 600, L131

Murray N., Quataert E., Thompson T. A., 2004, astro-ph/0406070

Murray S. D., Lin D. N. C., 1990, *ApJ*, 363, 50

Nagai D., Kravtsov A. V., 2003, *ApJ*, 587, 514

Navarro J. F., Frenk C. S., White S. D. M., 1997, *ApJ*, 490, 493

Navarro J. F., Steinmetz M., 2000, *ApJ*, 538, 477

Osmond J. P. F., Ponman T. J., 2004, *MNRAS*, 350, 1511

Ostriker E. C., 1999, *ApJ*, 513, 252

Pen U., 1999, *ApJ*, 510, L1

Prochaska J. X., Gawiser E., Wolfe A. M., Castro S., Djorgovski S. G., 2003, *ApJ*, 595, L9

Quinn T., Katz N., Efstathiou G., 1996, *MNRAS*, 278, L49

Rees M. J., Ostriker J. P., 1977, *MNRAS*, 179, 541

Ruszkowski M., Bruggen M., Begelman M. C., 2004, astro-ph/0403690

Scannapieco E., Oh S. P., 2004, *ApJ*, 608, 62

Schaye J., Aguirre A., Kim T., Theuns T., Rauch M., Sargent W. L. W., 2003, *ApJ*, 596, 768

Shapley A. E., Erb D. K., Pettini M., Steidel C. C., Adelberger K. L., 2004, *ApJ*, 612, 108

Shaviv N. J., Dekel A., 2003, astro-ph/0305527

Shen S., Mo H. J., White S. D. M., Blanton M. R., Kauffmann G., Voges W., Brinkmann J., Csabai I., 2003, *MNRAS*, 343, 978

Sheth R. K., Tormen G., 2002, *MNRAS*, 329, 61

Silk J., 1977, *ApJ*, 211, 638

Smail I., Ivison R. J., Blain A. W., Kneib J.-P., 2002, *MNRAS*, 331, 495

Somerville R. S., 2002, *ApJ*, 572, L23

Sutherland R. S., Dopita M. A., 1993, *ApJS*, 88, 253

Tasitsiomi A., Kravtsov A. V., Wechsler R. H., Primack J. R., 2004, *ApJ*, 614, 533

Thoul A. A., Weinberg D. H., 1995, *ApJ*, 442, 480

Thoul A. A., Weinberg D. H., 1996, *ApJ*, 465, 608

Tremaine S., Gebhardt K., Bender R., Bower G., Dressler A., Faber S. M., Filippenko A. V., Green R., Grillmair C., Ho L. C., Kormendy J., Lauer T. R., Magorrian J., Pinkney J., Richstone D., 2002, *ApJ*, 574, 740

Tremonti C. A., Heckman T. M., Kauffmann G., Brinchmann J., Charlot S., White S. D. M., Seibert M., et al., 2004, astro-ph/0405537

Voigt L. M., Fabian A. C., 2004, *MNRAS*, 347, 1130

White S. D. M., Frenk C. S., 1991, *ApJ*, 379, 52

White S. D. M., Rees M. J., 1978, *MNRAS*, 183, 341

Yan R., Madgwick D. S., White M., 2003, *ApJ*, 598, 848

Yang X., Mo H. J., van den Bosch F. C., 2003, *MNRAS*, 339, 1057

Zhao H., 2004, *MNRAS*, 351, 891

Zinger E., Birnboim Y., Dekel A., Kravtsov A., 2005, in preparation